Dear Editor and Reviewers:

Thank you very much for your comments on our manuscript [acp-2018-255]. We acknowledge the suggestions of two anonymous reviewers and are grateful to your efficient serving. We have updated the manuscript based on these valuable comments and suggestions, and the point-by-point responses are listed below.

Referee #1

General comments:

The authors focused on air quality along the Yangtze River based on a shipboard observation performed in winter of 2015. Over the past few decades, China's rapid development leads to huge cargo transports in the Yangtze River channel. However, there is lack of data for ship emission along the Yangtze River channel, especially in the inland area. From this viewpoint, this manuscript supplied value data and made some contributions to portray a picture of air pollution along the Yangtze River. However, the manuscript suffered from poor English written. There are a lot of wrong spelling, tedious sentence, vague expression. Generally, the manuscript is difficult to read and should be improved greatly before publication.

Response: Thank for reviewer's valuable comments. In the new version, we have updated the manuscript on the basis of the comments. Especially, we have improved the English presentation greatly, including grammar and typing mistake throughout the manuscript.

Specific comments:

1), Line 4 what mean "onboard and coastal areas".

Response: It means "people living along the Yangtze". This sentence has been changed to "Air quality over the Yangtze River is interesting as it may have significant influences on the aquatic ecosystem, the health of everyone living along the Yangtze River, and regional climate change."

2), Line 7 After the sentence of "Based on the filter samples,······", the PM$_{2.5}$ concentration

during the cruise campaign should be shown.

Response: We have added the PM$_{2.5}$ in Abstract. "The total average concentration of PM$_{2.5}$ were 119.29 ± 33.67 μg m^{-3}, and the dominate ionic composition in PM$_{2.5}$ was were SO$_4^{2-}$ with the average

concentration of 15.21 ± 6.69 μg m^{-3}, followed by one of NO_3^- (13.76 ± 4.99μg m^{-3}), NH_4^+ (9.38 ± 4.35μg m^{-3}), Ca^{2+}(2.23 ± 1.24μg m^{-3}) in this cruise."

3), Line 44-55 Authors cited a few of literatures focused on air quality on the region of Yangtze River Delta. In my opinion, authors should expand these literatures to the MLYR region, of which is overlapped well with the present region. Furthermore, the author should show specific regions shown in cited literatures.

Response: This was changed. To best our knowledge, numerous studies have been conducted in megacities in the MLYP region, especially Nanjing and Shanghai. Of course, there are also many papers which were related to air quality in other cities or rural in YRD region. However, we still thought long-time observation and sampling on air quality were only focused in Nanjing and Shanghai.

4), Line How about the T/B values for EP3 and EP5?

Response: We have re-calculated our data, and new results have been changed in the new manuscript in Table 2. Air mass with T/B ratio ≥ 2 were identified from fresh emissions. As shown in Figure S2, the peak value of T/B ratio clearly performed in EP-3 and EP-5, suggesting fresh emission dominant.
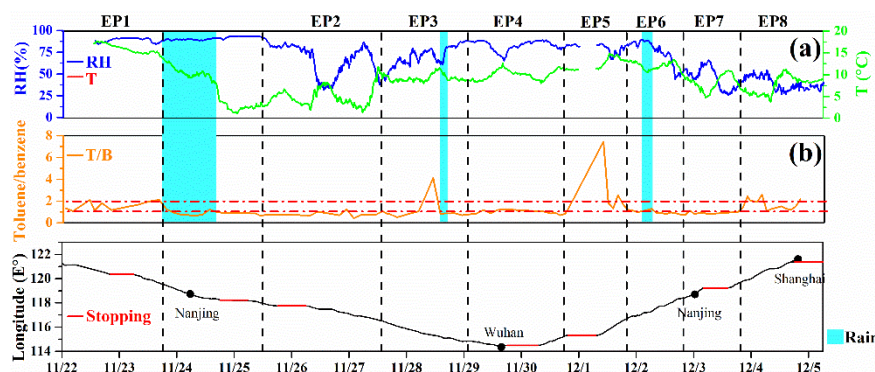
Figure S2. Time series of meteorological parameters during YRC (T and RH). (b) Time series of ratio of Toluene to Benzene.

5), Line 214 there are two "with". This sentence should be written.

Response: This sentence has been changed to "The local air during EP-4 was in low pressure system with low wind speeds that didn't favor the diffusion of the local pollution".

6), Line 292-293 "……, accounting for 37.43% and 40.15% in PM$_{2.5}$ and PM$_{1.0}$?", gained in the present study?

Response: Yes, these data all acquired from this cruse. This sentence has been changed to "……, accounting for 37.43% and 40.15% in $PM_{2.5}$ and $PM_{1.0}$ during YRC, respectively"

5, Line 462 "……and the YDR, Jiangsu, east of Anhui, and the Mongolian plateau were identified as the major source regions, and pathways." This sentence should be rewritten.

Response: this sentence has changed to "Fine particles Ni (Figure 6i) had almost same spatial distribution with Cr, that Shanghai, Jiangsu, and East of Anhui, and the Mongolian plateau were identified as the major potential source regions or pathways, owing to ship emissions, nonferrous metal mining, and smelting industries. The Mongolian plateau also was a source region, indicating that nature dust may be possible source for Cr and Ni."

Technique corrections:

(1) Line 3 "River" is changed to be "river".

(2) Line 11 "the secondary inorganic formation" should be changed to "the secondary inorganic aerosol formation".

(3) Line 19 "This result……"should be changed to "The results".

(4) Line 35 "their effects" should be changed to "their negative effects".

(5) Line 40 "……and possible sources in this region have been generally characterized" should be changed to "……and source identification in this region have been generally studied".

(6) Line 63 "The MLYR" should be changed to "The MLYR region", and "effecting its air quality" should be deleted.

(7) Line 68 "particle matter" should be abbreviated to be "PM".

(8) Line 77 "noted" should be changed to "pointed out".

(9) Line 79 "Shanghai port" should be changed to "The Shanghai port".

(10) Line 83 "the air quality" should be changed to "air quality".

(11) Line 93 "to the best of our knowledge, it is the first systematic observation to characterize the air pollution along the China's largest and longest river" should be changed to "to the best of our knowledge, it is the first systematic observation on air pollution along the Yangtze River".

(12) Line 97 "A mobile haze monitoring platform" should be changed to "A mobile monitoring platform".

(13) Line 204-205 A sentence should be added here to explain the T/B value for weather

identification, although it has been explained in the Experimental section.

(14) **Line 206 "supplements" should be changed to "supporting information".**

(15) **Line 217 "in the sixth episode" should be changed to "For the sixth episode".**

(16) **Line 233 "Their detail information" should be changed to "The detailed information".**

(17) **Line 245 "......, mainly owing to local emissions, photochemical processes and meteorology conditions (Xu et al., 2011)" should be deleted.**

(18) **Line 247 "cities" was changed to "the cities".**

(19) **Line 252 "was substantially enhanced" should be changed to "increased".**

(20) **Line 261 "the mean levels" should be changed to "the mean level".**

(21) **Line263 "revealed" should be changed to "was characterized by".**

(22) **Line 264 "edge" should be changed to "banks".**

(23) **Line 266 "by" should be changed to "identified by".**

(24) **Line 268 "regionally" should be changed to "apparently".**

(25) **Line 430 "the similar source region distributions" should be changed to "the similar region distributions".**

(26) **Line 542 "It is noted that" should be changed to "It was noted that".**

(27) **Line 564 "the YRD regions" should be changed to "the YRD region".**

(28) **Line 567 "Ship engine emission" should be changed to "Ship emission".**

Response: We have followed these valuable suggestions and made the corrections accordingly.

Referee #2

General comments:

General comment: This manuscript aims to provide a good picture of air pollution in the Mid-Lower Reaches Yangtze River (MLYR) based on a 15-day cruise campaign in winter of 2015. With chemical speciation data from filter samples, sources impacting the MLYR region are discussed including coal combustion, ship emission, biomass burning etc. Although these are important data, there are still some limitations of this work. One is the number of samples is limited, and the other is that in the data analysis section, it is pretty descriptive. Instead, there should be more in-depth discussion and it should be more logic and structured. With the current information provided in

the manuscript, it is hard to draw firm conclusions. Therefore, I suggest the authors to revise the manuscript with in-depth data analysis and provide clear and new conclusions.

Response: We thank the reviewer for their helpful comments and suggestions, which are helpful for the improvement of the manuscript. We also have in-depth re-analyzed our data and revised the manuscript carefully according to the reviewer's comments.

Specific comments:

1). Why is levoglucosan from satellite data instead of from filter samples? What about the spatial resolution of satellite data? The authors indicate that biomass burning may make a big contribution to rural area. It will be more interesting to know the quantitative contribution from biomass burning.

Response: Thank for reviewer's valuable comments. The mass concentration of levoglucosan were analyzed from filter samples ($PM_{2.5}$) by IC methods. We just acquired the value aerosol optical depth (AOD), and SO_2, CO, NO_2 column concentration from Satellite data. We have added spatial resolution of satellite datasets in section 2.4. "Based on spatial interpolation methods, all of data from satellite datasets were interpolated and averaged into grid cells with a $0.25° \times 0.25°$ resolution".

Thank you for interesting in biomass burning event in rural region along over MLYP region. As you suggested, we also try to quantify the contribution of biomass burning to particulate matter. In general, both K^+ and levoglucosan (lev) could be regarded as tracers for biomass burning. However, significantly correlation between Ca^{2+} and K^+ suggested that dust could be the major source of K^+ in $PM_{2.5}$ sampled during YRC. Meanwhile, numerous studies have confirmed that lev mostly originate from biomass burning. Hence, the levoglucosan concentration and ratio of OC to lev (OC/lev) were widely used to estimate the contribution of biomass burning to organic carbon. The detailed information will be added in section 3.4.4 "The levoglucosan concentration and ratio of OC to lev (OC/lev) were widely applied to estimate the contribution of biomass burning to organic carbon in $PM_{2.5}$. To further quantify the contribution of biomass burning to OC, an empirical model was utilized as proposed by Wan et al. (2017):

$$OC_{BB} = (\frac{[lev]}{[OC]})_{ambient}/(\frac{[lev]}{[OC]})_{BB} \quad (5)$$

The differences of the (lev/OC) $_{BB}$ ratio among different biomass fuels and combustion conditions were taken into account. So, the average (lev/OC)$_{BB}$ ratio of 8.14 % was selected to calculate the contribution

of BB to OC (Wan et al., 2017). Figure S9 presents the variation of lev/OC ratio along the Yangtze River. The ratio of lev/OC during this cruise ranged from 0.03 % to 0.91 % with an average of 0.35 ± 0.24 %, which was comparable to that of Lin'an in YRD region (Liang et al., 2017). However, the ratio of lev/OC during YRC was near an order of magnitude of lower than its value in New Delhi (3.1 ± 0.8 %) (Li et al., 2014) and Lumbini (3.34 ± 2.53 %) in the northern edge of Indo-Gangetic Plain (Wan et al., 2017), where BB play an important role on air quality. Figure S9 also shows the time serious of contribution of BB-OC to OC. The average contribution of BB-OC/OC was 4.26 ± 2.89 %, while the mean mass fraction of OC to $PM_{2.5}$ was slightly higher than 20%.The peak contribution of OC deriving from BB to total OC of $PM_{2.5}$ nearly accounted for 11% in EP-6, which was approached that of the Pearl River region sites (13%) (Ho et al., 2014). Here, it's emphasized that our method based on empirical formula and value is just rough estimation. Hence, the radiocarbon measurement (^{14}C) of carbonaceous aerosol and air quality model simulation should need to confirm this result in the future.

Figure S9. Time serious of Lev/OC and Lev/$PM_{2.5}$ ratios, and contribution of BB-OC to OC and $PM_{2.5}$ during YRC.

2). The influence of ship emission on $PM_{2.5}$ in urban city is an important question. The authors claim that the ship plume could contribute to more than 50% of the total $PM_{2.5}$ in the Shanghai ports. As there are quite a few assumptions, how to validate such result (50% of the total $PM_{2.5}$)?

Response: Thank for reviewer's valuable comments. As your stated above, the ship emissions have become an important pollution sources in the port cities. The Yangtze River Campaign give us a valuable opportunity to study ship emissions along the biggest and busiest river in China. In present study, we try to evaluate and quantify ship emissions along Yangtze River. Firstly, the emission factors of heavy metal from four different oil were analyzed in our lab. V are only detected in heavy oil. Although both Ni and V were frequently regarded as tracers for heavy oil, only V was selected as a tracer for heavy fuel oil in

present study. Next, the primary ship emissions were re-analyzed and calculated. It was presented in section 3.5.1. However, numerous studies also pointed out that this method underestimate the contribution of ship emissions, due to lack of rare elements such as:Tb, Er, Yb, and Lu. Besides, ship plume also released larger amount of NO_X, SO_2, and VOCs, which all are precursors for secondary aerosol. Hence, we try to access the contribution of ship emissions to secondary aerosol. The limit ratio of SO_4^{2-}/V, NO_3^-/V, and OC/V were used to evaluate the SO_4^{2-}, NO_3^-, and OM from ship emissions. We thought it is still reliable method to estimate the concentration of sulfate and OM deriving from HFO ship emissions. However, chemical process of NO_X to nitrate is complex and contribution nitrate originating from ship emissions were high variable. Recently, many studies have verified that nitrate has become dominant components in $PM_{2.5}$ collected in Shanghai. Hence, other mobile sources (except ship emissions) also may be important sources for nitrate in $PM_{2.5}$. "However, it is worth noting that our estimation based on empirical values were limited by meteorological conditions and sample numbers. Hence, long-term observation and high resolutions model simulation of ship emissions should be strengthened along the Yangtze River, especially in Shanghai harbor clusters."

3). There are many typos in the manuscript and it requires careful revision. It is clear that there is a need to improve English in the manuscript.

Response: Thank your valuable suggestion. In the new version, we have improved the English presentation greatly, including grammar and typing mistake throughout the manuscript.

Reference:

Ho, K. F., Engling, G., Sai Hang Ho, S., Huang, R., Lai, S., Cao, J., and Lee, S. C.: Seasonal variations of anhydrosugars in $PM_{2.5}$ in the Pearl River Delta Region, China, Tellus B: Chemical and Physical Meteorology, 66, 22577, 10.3402/tellusb.v66.22577, 2014.

Li, J., Wang, G., Aggarwal, S. G., Huang, Y., Ren, Y., Zhou, B., Singh, K., Gupta, P. K., Cao, J., and Zhang, R.: Comparison of abundances, compositions and sources of elements, inorganic ions and organic compounds in atmospheric aerosols from Xi'an and New Delhi, two megacities in China and India, Sci. Total Environ., 476-477, 485-495, 10.1016/j.scitotenv.2014.01.011, 2014.

Liang, L., Engling, G., Zhang, X., Sun, J., Zhang, Y., Xu, W., Liu, C., Zhang, G., Liu, X., and Ma, Q.: Chemical characteristics of $PM_{2.5}$ during summer at a background site of the Yangtze River Delta in China, Atmos. Res., 198, 163-172, 2017.

Wan, X., Kang, S., Li, Q., Rupakheti, D., Zhang, Q., Guo, J., Chen, P., Tripathee, L., Rupakheti, M., Panday, A. K., Wang, W., Kawamura, K., Gao, S., Wu, G., and Cong, Z.: Organic molecular tracers in the atmospheric aerosols from Lumbini, Nepal, in the northern Indo-Gangetic Plain: influence of biomass burning, Atmos. Chem. Phys., 17, 8867-8885, 10.5194/acp-17-8867-2017, 2017.

Air quality in the middle and lower reaches of the Yangtze River channel: A cruise campaign

Zhong Li[1], Chunlin Li[1,2], Xingnan Ye[1], Hongbo Fu[1], Lin Wang[1], Xin Yang[1], Xinke Wang[3],Zhuohui Zhao[4], Haidong Kan[4], Abdelwahid Mellouki[5], Jianmin Chen[1,4,*]

[1] *Shanghai Key Laboratory of Atmospheric Particle Pollution and Prevention, Fudan Tyndall Center, Department of Environmental Science & Engineering, Institute of Atmospheric Sciences, Fudan University, Shanghai 200433, China*

[2] *Department of Earth and Planetary Sciences,Weizmann Institute of Science*

[3] *Univ Lyon, Université Claude Bernard Lyon 1 CNRS, IRCELYON, F-69626, Villeurbanne, France*

[4] *School of Public Health, Fudan University, Shanghai 200032, China*

[5] *Institut de Combustion, Aérothermique, Réactivité et Environnement, CNRS, 45071 Orléans cedex 02, France*

[*]**Correspondence to:** Jianmin Chen (jmchen@fudan.edu.cn)

1   **Abstract**

2   Yangtze River is the longest river in China, nearly one-third of the national population lives along the

3   river. Air quality over the Yangtze River is interesting as it may have significant influences on the aquatic

4   ecosystem, health of everyone living along the Yangtze River, and regional climate change. Chemical

5   compositions of ambient aerosol were determined during a comprehensive cruise campaign carried out

6   along the Mid-Lower Reaches Yangtze River (MLYR) in winter of 2015. The total average concentration

7   of $PM_{2.5}$ were 119.29 ± 33.67 μg m^{-3}, and the dominate ionic composition in $PM_{2.5}$ was were SO_4^{2-} with

8   an average concentration of 15.21 ± 6.69 μg m^{-3}, followed by NO_3^- (13.76 ± 4.99 μg m^{-3}), NH_4^+ ($9.38 \pm$

9   4.35 μg m^{-3}) and Ca^{2+} (2.23 ± 1.24 μg m^{-3}) in this cruise. Based on the filter samples, the concentration and

10   chemical composition of $PM_{2.5}$ were remarkably varied or fluctuated from coastal areas to inland over

11   the MLYR region. Crustal elements (Ca, Mg, Al and K) from floating dust showed peak concentrations

12   in the Yangtze River Delta (YRD) region, while secondary inorganic species (SO_4^{2-}, NO_3^- and NH_4^+) and

13   some most enriched elements (Pb, As, Se and Cd) presented the high levels in central China (Wuhan

14   region). The significant correlation between Se and SO_4^{2-} suggested that coal combustion may play an

15   important role in secondary inorganic aerosol formation. The relative high enrichment factors (EFs) of

16   Ca (EFs > 100) suggested the crustal elements may derive from anthropogenic sources. Furthermore, the

17   concentration of levoglucosan in $PM_{2.5}$ and CO column level from satellite observation greatly enhanced

18   in the rural areas (Anhui and Jiangxi), indicating that biomass burning may make remarkable contribution

19   to the rural area. The concentrations of typical tracer for heavy oil (V and Ni) significantly increased in

20   the Shanghai port, that was mainly ascribed to the ship emission, based on the air mass source analysis

21   and the relatively high ratio of V/Ni as well. The results shown herein portrayed a good picture of air

22   pollution along the Yangtze River.

23   **Keywords:**

24   Shipboard observation, chemical composition, ship emission, Yangtze River

25   **1 Introduction**

26   Yangtze River is the longest river in China, originating from the Qinghai-Tibetan Plateau and extending

27   to the East China Sea, and it drains an area of 18,08,500 square km basin, of which is China's great

28   granary, and feeds nearly one-third of the national population (Liu et al., 2007; Jiang et al., 2008).

29   Currently, three densely city agglomerations, including Wuhan, Nanjing, and Shanghai (WNS), which

are the centers of economy, transportation, politics, and culture in central and eastern China, and all of which are home to larger petrochemical complex and/or steel industry, have formed along both shores of the Mid-Lower Reaches Yangtze River (MLYR). The MLYR region is one of the most developed and economically vibrant regions in China, accounting for 34.13% of China's total GDP in 2015. Owing to fast economic development and industrialization, this region has become one of the most polluted areas in China (Xu et al., 2016b).

Fine aerosol particles are becoming more important in recent years, due to their negative effects on human health, agriculture, and climate change (Wang et al., 2012; Kang et al., 2013b; Pöschl, 2005; Seaton et al., 1995; Ackerman et al., 2004; Stier et al., 2005; Chameides et al., 1999; Novakov and Penner, 1993; Jones et al., 1994). Numerous field observations related to fine particles have been conducted in the megacities in the Yangtze River Delta (YRD) region, especially in Nanjing and Shanghai. Over the past years, the variation of mass concentrations, chemical compositions, size distributions, seasonal variations, daily change, optical properties, and temporal-spatial distributions of fine particles in this region have been investigated, and the causes and impacts of aerosol pollution have also been generally studied (Zhou et al., 2016; Kang et al., 2013b; Tao et al., 2014b; Shen et al., 2014; Fu et al., 2014; Huang et al., 2013; Huang et al., 2012b; Huang et al., 2012a; Ding et al., 2013a; Ding et al., 2017; Zhang et al., 2010). By analysis of several serious haze cases, Huang et al. (2012) pointed out that secondary inorganic and dust episodes always erupted in spring, while biomass burning (BB) event was often observed in summer (harvest season for wheat). Further, the high sulfate oxidizing rate (SOR) and nitrate oxidizing rate (NOR) were also observed from long-term field measurements in Nanjing and Shanghai, indicating that photochemical reactions in the atmosphere were quite active in these areas (Zhou et al., 2016; Zhou et al., 2017; An et al., 2015). Wang et al. (2015b) also found that secondary pollutants contributed the major fraction of aerosol mass, especially in Shanghai-Nanjing city cluster. The increasing trend of the NO_3^-/SO_4^{2-} rations since the year 2000 suggested that vehicle sources became more important in this region (Kang et al., 2013a; Huang et al., 2012a; Tao et al., 2014b; Sun et al., 2017). Beyond, Cheng et al. (2014) estimated that BB contributed 37% of $PM_{2.5}$, 70% of organic carbon, and 61% of element carbon in harvest, respectively. If BB was controlled and even forbidden in this season, the $PM_{2.5}$ levels would decrease by 47% in the YRD region (Cheng et al., 2014). Some typical events, including fresh combustion pollution from firework (Zhang et al., 2010; Kong et al., 2015), and the peak of secondary inorganic aerosol species (SNA, SO_4^{2-}, NO_3^-, and NH_4^+) deriving from the travel rush and re-opening of

factories after China Spring Festival (Huang et al., 2012b; Kong et al., 2015), have also been focused and analyzed. Huang et al. (2013) also investigated the chemical composition of fine particles in Shanghai, finding that the concentrations of anthropogenic calcium drastically decreased as results of strict monitoring and implementing control of construction activity during 2010 Word Expo. Compared with normal (pre-control) periods, the levels of Ca^{2+} and SO_2 also reduced 55% and 46% during the 2014 Youth Olympic Games, respectively (Zhou et al., 2017).

The MLYR region faces the most complex anthropogenic emission sources, including a variety of power plants, large petrochemical and steel industries, and farmland distributed along both banks of the Yangtze River, as well as ship emissions. It was well documented that ship emissions displayed a significant impact on regional air quality, particularly in traffic hubs and harbors (Pandis et al., 1999; Becagli et al., 2017; et al., 2014). The contribution and effect of ship emissions to local air pollution, especially PM, have been briefly analyzed at levels from regional to global (Jalkanen et al., 2015; Zhan et al., 2014; Pandis et al., 1999; Fan et al., 2016; Coggon et al., 2012). The emission factors, and properties of emitted particles and gases from ship-plume in different engine speeds were also reported (Zhang et al., 2016; Moldanová et al., 2009; Agrawal et al., 2009). Ship-related pollutants have been identified in the YRD port cluster and surrounding area. In 2010, SO_2, NO_x, and $PM_{2.5}$ from ship emissions in the YRD port cluster were up to 3.8×10^5 t/y, 7.1×10^5 t/y, and $5.1 \times$ t/y, respectively. The maximum SO_2 and NOx concentrations from ship emissions in harbors or traffic hubs were nearly 36 times and 17 times higher than the maximum land-based emissions, respectively (Fan et al., 2016). Zhao et al. (2013b) pointed out that Ni and V enriched in submicron particles in Shanghai port. Recently, Liu et al. (2017) also reported that ship-plume contributed to 2-7 $\mu g\ m^{-3}$ to fine particle within the coastal of Shanghai port, accounting for 20-30% of total $PM_{2.5}$. Known as "golden canal", Yangtze River was an important route for trade and travel. However, there is seldom data related to air quality and the influence of ship emissions along the Yangtze River channel. Meanwhile, related observations with the synchronous trend of aerosol in the MLYR region remain insufficient.

To characterize air quality in this region, a round-trip field observation voyage, namely Yangtze River Campaign (YRC), was carried out between Shanghai and Wuhan. This cruise aimed to characterize the chemical components of atmospheric pollutants, to analyze these spatial distributions, and to identify potential source contribution. To the best of our knowledge, it is the first systematic observation on air pollution along the largest and longest river in China.

2 Measurements and methods

2.1 Overview YRC

A mobile monitoring platform (A container: length 10.0 m, width 4.0 m, and height 2.5m) was placed on a vessel (length: 20 m, width 6 m), sailing from 22 November to 05 December in 2015 along the Yangtze River channel between Shanghai to Wuhan (29.72°N-32.33°N, 114.33°E-121.61°E). This campaign route is illustrated in Figure 1. Starting on 22 November in the Waigaoqiao port of Shanghai, then the vessel crossed Jiangsu, Anhui province, and finally arrived at the Hankou port in Wuhan, Hubei province on 29 November along the Yangtze River waterway. The ship shifted at an average speed of 1 m/s heading the upper the Yangtze River towards Wuhan. After berthing in the port of Wuhan one night, the vessel turned around, departed, and shifted towards Shanghai. This cruise finally ended in the Waigaoqiao port in Shanghai on 5 December. During YRC, a wide range of data, including common meteorological parameters, trace gas concentrations (CO, NO-NO_x, SO_2, and O_3), chemical composition of aerosol particles, and satellite dataset over this region were acquired and analyzed.

2.2 Trace gases measurements

A serious of commercial trace gas instruments, including 43i SO_2 analyzer, 48i CO analyzer, and 42i NO-NO_2-NO_x analyzer (Thermo Environmental Instruments Ins., USA C-series), were installed in an air-conditioned container to measure the concentration of gaseous pollutants. The routine procedures of QA/QC (the daily zero/standard calibration) were performed, according to the technical guidance by U.S. Environmental Protection Agency (USEPA, 1998).

Trace alkanes, including toluene and benzene, were also sampled in stainless summa canister, and quantified by a gas chromatograph with a mass spectrometer and a flame ionization detector (GC-MS/FID) (Wang et al., 2014). The sampling interval of VOCs was 3 hours with fluctuation. The ratio of toluene/benzene (T/B) was commonly regarded as an indicator of the photochemical processing (Baltrenas et al., 2011). The high ratio of T/B indicated that air masses were fresh emissions, while lower value suggested that air masses had undergone photochemical processes. In this paper, we used the same value ratio of T/B in CalNex (Gaston et al., 2013). Air masses with T/B << 1 were excepted to well undergo photochemical aging while urban fresh air masses had much higher T/B ratio (≥2). Ship track self-emission was removed by subducting the periods when the winds blew from the stern, that is, the

118 relative wind direction was from 130˚ to 220˚ to the ship direction (0˚ in the front). The real-time

119 measurement of trace gases and aerosol data presented here were filtered out by this method.

2.3 Chemical analysis of the filter samples

121 Particulate samples of $PM_{2.5}$ and $PM_{1.0}$ were simultaneously collected on separate quartz filters (Φ90 mm,

122 Whatman Inc., Maidstone, UK) using a medium-volume sampler by HY-100 (Qingdao Hengyuan S.T.

123 Development Co., Ltd, China) (model: $PM_{2.5}/PM_{1.0}$; flow rate: 100 L min^{-1}, respectively), which was

124 placed on the foredeck at approximately 3.0 m above sea level. The duration time of collecting sample

125 was generally set at 12 h (in parallels: day 07:00-19:00, night 19:00-07:00), while it was also collected

126 PM for 24 h. High-purity quartz filters were preheated at 500 ℃ for 10 h to virtually eliminate the

127 residues prior to sampling. All the samples were stored in a refrigerator keeping at -20 ℃ for analysis.

128 The filter sample masses were measured by an intelligent weight system (Hangzhou Wmade Intelligent

129 Technology co., LTD) which was maintained in constant condition (Temperature (T): 20 ℃ and

130 Relative humidity (RH): 40%). All the procedures were well documented, and supervised to avoid the

131 possible contaminations. The sample instruments were placed on the bow of the ship far away from its

132 track. Ship self-emission in the filter samples was ignored, since the most prevailing winds blew from

133 the bow to the stern during the sampling periods.

134 One-eighth of each filter was extracted ultrasonically by 20 mL of deionized water (18.2 MΩ cm^{-1})

135 for 40 min. After filtering, eight inorganic ions (SO_4^{2-}, NO_3^-, Cl^-, NH_4^+, Na^+, K^+, Ca^{2+}, and Mg^{2+}) were

136 analyzed by an ion chromatography (940 Professional IC, Metrohm, Switzerland), and a sugar column

137 coupled with pulsed electrochemical detection (945 Professional Detector Vario, Metrohm, Switzerland)

138 was used to measure levoglucosan (lev) in the extract. Both of instruments were controlled with a IC

139 software. The lower and upper limits of the detection were 0.5 and 4 μg m^{-3}, respectively. The relative

140 standard deviation of each ion was less than or equal to 2% from three reproducibility tests. Blank

141 samples were analyzed with the same processes to remove potentially contaminations.

142 One-eighth of the sample filter and the blank filter were cut into fragments, and digested at 170 ℃

143 for 4 h in a high-pressure Teflon digestion vessel with 3 mL of HNO_3 and 1 mL of $HClO_4$ (Wang et al.,

144 2006; Li et al., 2015b). After cooling, the digested solution was filtered and diluted to 15 mL with

145 ultrapure Mill-Q water. An inductively coupled plasma mass spectrometer (ICP-MS, Agilent 7500a) was

146 employed to measure the concentrations of 17 elements (Al, As, Ca, Co, Cr, Cu, Fe, K, Mg, Mn, Na, Ni,

147 Se, Tl, Pb, V, and Zn) in the filter samples. National standard material (soil, GSS-12, China) was also

148 digested, and used to calculate the element recoveries ranging from 91%-102%. The detection limits of

149 the trace elements were derived from the standard deviation (3δ) of the blank values. Details relating to

150 ICP-MS have been described in elsewhere (Li et al., 2015b).

151 Organic carbon (OC) and elemental carbon (EC) in the aerosol samples were analyzed by a

152 Thermal/Optical Carbon Analyzer (DRI Model 2001). Each sample was identified as four OC fractions

153 (OC1, OC2, OC3, and OC4 at 120, 250, 450, and 550 ℃, respectively, in a helium-air) and three EC

154 fractions (EC1, EC2, and EC3 at 550,700, and 800 ℃, respectively, in the mixture air (98% helium and

155 2% oxygen) by an IMPROVE thermal/optical reflectance (TOR) protocol. Pyrolyzed organic carbon

156 (POC) was separately detected by transmittance. IMPROVE OC was defined as OC1 + OC2 + OC3 +

157 OC4 + POC, and EC was calculated by EC1 + EC2 + EC3 − POC.

158 **2.4 Satellite data and ship traffic data**

159 The satellite databases, including Moderate Resolution Imaging Spectroradiometer (MODIS) with a

160 resolution of 10×10 km, Measurement of Pollutants in the Troposphere (MOPITT) and Ozone

161 Monitoring Instrument (OMI) on the National Aeronautics reaching a spatial resolution of 13×24 km at

162 nadir, and Space Administration's Earth Observing System (NASA's EOS) Aura satellite, were applied

163 to provide spatial distribution of aerosol particles and trace gases (Xu et al., 2011; Huang et al., 2012a).

164 The column levels of CO, NO_2, SO_2, and aerosol optical depth (AOD) were retrieved over the MLYR

165 region. In this study, all of data from satellite datasets were interpolated and averaged into grid cells with

166 a $0.25° \times 0.25°$ resolution.

167 Ship positions and numbers in the Yangtze River channel were decoded by Automatic Identification

168 System (AIS) databases which were obtained from the Marine Department. A 15-day AIS datasets along

169 the Yangtze River were selected with a high time resolution (about 15min).

170 **2.5 Potential source contribution function**

171 The potential source contribution function developed by Hopke et al. (1995) was applied to derive the

172 potential source regions and spatial distributions. In this study, 3 day back trajectories arriving at height

173 of 500 m was calculated using National Oceanic and Atmospheric Administration's (NOAA's) Hybrid

174 Single Particle Lagrangian Integrated Trajectory (HYSPLIT-4) model (http://www.arl.noaa.gov/ready/

175 open/hysplit4.html) with global meteorological data from NCEP reanalysis data (ftp://arlftp.arlhq.noaa.

176   gov/pub/archives/rean-alysis) (Draxler and Hess, 1998). The contribution of the potential sources during

177   YRC was calculated by the PSCF analysis with TrajStat (Wang et al., 2009). The domain sources were

178   restricted to 25°N‑45°N and 110°E‑125°E, which were divided into grid cells with a 0.5°×0.5° resolution.

179   The PSCF value for the ij th grid cell was defined as:

180    $$\text{PSCF}_{ij} = \frac{M_{ij}}{N_{ij}} W_{ij}(1)$$

181   where N_{ij} is the total number of trajectory segment endpoints that fall in the ij cell, and M_{ij} is the

182   number of endpoints for the same cell with arrival times at the sampling site, corresponding to pollutant

183   concentrations higher than an arbitrary criterion value. In this study, the average concentration for each

184   trace element was set as the criteria value. To reduce the random error and uncertainty of the small value

185   of n_{ij}, the weighting function of W_{ij} reduced the PSCF values when the total number of the endpoints

186   in a particular cell n_{ij} was less by approximately 3 times than the average N_{Ave} value of the endpoints

187   per each cell (Han et al., 2005):

188    $$W_{ij} = \begin{cases} 1.00 & N_{ij} > 3N_{Ave} \\ 0.70 & 1.5N_{Ave} < N_{ij} \leq 3N_{Ave} \\ 0.42 & N_{Ave} < N_{ij} \leq 1.5N_{Ave} \\ 0.17 & 0 < N_{ij} \leq N_{Ave} \end{cases} (2)$$

189   **3 Results and discussion**

190   **3.1 Classification of the typical pollution episodes**

191   The air pollution during the cruise was classified into eight distinct episodes, based on sampling locations,

192   backward trajectories, and photochemical processes (T/B value) (Figure 1, Figure S1, Figure S2 and

193   Table 1). The detailed meteorological information over the MLYR region was also summarized in the

194   supporting information. As shown in Figure S1, the first episode (EP-1), starting from 22 to 23 November,

195   was characterized by the sampled air masses which came from the East China Sea, and were typically

196   influenced by the local industry and Shanghai harbor pollution. The ratio of T/B ranged from 0.6 to 2

197   with an average of 1.3, suggesting fresh air masses mixed by the aged ones. The air masses in the

198   secondary episode (EP-2), with B/T<1, originated from the rural areas (Anhui and Henan), carrying

199   agriculture emission (Figure S2). Sampled air masses stagnated around Jiujiang to Wuhan from the third

200   episode (EP-3) to the fifth episode (EP-5). However, the fourth episode (EP-4) (Wuhan region) with the

201   low average T/B ratio of 0.97 undergone well atmospheric aging. The local air during EP-4 was in low

pressure system with low wind speeds that didn't favor the diffusion of the local pollution (Figure S3). Air mass with T/B ratio $\geqslant$ 2 were identified from fresh emissions. Both EP-3 and EP-5 (nearly Jiujiang) were characterized by high T/B value (Figure S2), suggesting that these two pollution episodes were contributed mainly from regional fresh emissions. For the sixth episode (EP-6), the wind direction shifted from southwest to northwest, and the vessel was again traveling through the rural area of middle reach of Yangtze River, suggesting that air masses may originate from agricultural activities. Then in the seventh episode (EP-7), a cold front arrived, and wind speeds increased significantly from average 3.84 m/s to 5.38 m/s (Table 2) with air masses transported from northern inland regions, which was further confirmed by wind fields (Figure S3) and the sharply decreases of RH (Table 2). The last episode (EP-8) was in the YRD region where highly intensive anthropogenic activities released a large amount of the pollutants. Air masses in EP-8, with the average T/B value of 1.73, were expected to mixture of aged masses sources with regional fresh emissions. Overall, EP-1 and EP-8 (the YRD region) were mainly influenced by fresh local emissions mixed with aged air masses, while agriculture emissions contributed significantly during EP-2 and EP-6 episodes. Both EP-3 and EP-5 were characterized by fresh emissions, even though the megapolis was not available in this region. The cruise started on November 22, but the offline $PM_{2.5}$ samples were collected after November 25. Thus, EP-1 description was ignored in the present study.

3.2 Air pollution during YRC

3.2.1 Variability of air pollutants observed in the vessel

The $PM_{2.5}$ and $PM_{1.0}$ was sampled from 25 November to 5 December in 2015. The detail information is also summarized in Table 1. The average mass concentrations of $PM_{1.0}$ and $PM_{2.5}$ during YRC were 96.69 $\pm$ 22.18 $\mu g\ m^{-3}$ and 119.29 $\pm$ 33.67 $\mu g\ m^{-3}$, respectively. The average ratio of $PM_{1.0}/PM_{2.5}$ was 0.8 $\pm$ 0.085, implying that $PM_{2.5}$ mainly dominated by fine particles with the size of < 1.0 μm. The detailed meteorological information, including T, RH, pressure, wind direction and wind speed, and trace gaseous in different episodes are also summarized in Table 2. The peak concentrations of $PM_{2.5}$ were observed in EP-4 and EP-7 (Table 1). However, there were obvious differences between EP-4 and EP-7 in the meteorological parameters and trace gases levels, indicating that these two pollution events were completely different. As mentioned in 3.1, sampled air masses in EP-4 mainly originated from local emissions, whereas EP-7 was influenced by a long-transport of air pollution.

231   As shown in Table 2, the average concentrations of CO, SO_2, and NO_X varied dramatically in the

232   different pollution episodes. Average concentrations of CO, and SO_2 (993.96 ± 387.34, and 9.32 ± 4.33

233   ppbv, respectively) were slightly lower than those in the cities in winter, including Wuhan (1024.00, and

234   13.30 ppbv) (Wang et al., 2017), Nanjing (1096.00, and 13.09 ppbv) (Sun et al., 2017), Chengdu (1440.00,

235   and 12.60 ppbv) (Liao et al., 2017), and Shanghai (1067.20, and 18.90 ppbv) (Huang et al., 2012a). CO

236   level continued to rise since the start of the YRC, and finally peaked in EP-6 and EP-7. Meanwhile the

237   SO_2 and NO_X levels were much lower in these two episodes, which were identified as the BB event. As

238   previously reported, biomass burning could produce large amount of CO, while NO_X and SO_2 were not

239   the major gaseous pollutants released from BB (Huang et al., 2012a; Ding et al., 2013b). The mean CO

240   concentration in EP-7 reached to 1224.88 ppbv, which was close to the level recorded at Shanghai during

241   the harvest season of wheat (June) (Huang et al., 2012a). The SO_2 concentrations in EP-3 and EP-8

242   greatly increased, which were close to the SO_2 level in the haze event in Shanghai (Huang et al., 2012a).

243   This was partly caused by local fresh emissions (the high T/B in EP-3 and EP-8). Except for EP-6 and

244   EP-7 (BB event), the NO_X concentration almost exceeded 50 ppbv along this cruise. The average mass

245   concentration of NO_x in this cruise is 63.74 ± 41.08 ppbv, which was much higher than the mean level in

246   Shanghai (42.40ppbv, 2012) (Han et al., 2015), and Guangzhou (39.14ppbv, 2012) (Zou et al., 2015) that

247   represented typical urban NO_X level. The NO_X concentration peaked in EP-3, which was identified to

248   mainly come from local emissions. The high NO_X level along YRC was identified to come from strong

249   regional emission. It could be derived that multiple sources of air pollution distributed on both banks of

250   the Yangtze River.

251   **3.2.2 Regional distribution of air pollutants identified by remote sensing observation**

252   The MLYR region is one of the most polluted areas in China, and the spatial distribution of various

253   pollutants were apparently different from coastal to inland region. As shown in Figure 2a, the high

254   average values of AOD retrieved from MODIS MOD04 were observed in eastern Jiangsu and Shanghai,

255   etc, where human and industrial activities were concentrated, suggesting that anthropogenic emissions

256   were dominated. However, there was much missing data of AOD in central China due to heavy clouds.

257   As presented in Figure S4 of the MODIS true-color imagery on 28 November, thick clouds covered

258   across central China. Besides, the average of AOD was about 0.45, which was slight lower than that in

259   Shanghai in winter (0.55) (He et al., 2012), and background (0.65) in the North China plain (Xu et al.,

260   2011). The AOD value in northern China was higher than that in southern China. As plotted in Figure

2b, CO surface mixing ratio calculated by MOPITT revealed that Shandong, Henan, and Anhui were exposed to elevated CO column concentrations. CO is an important tracer for the incomplete combustion sources, such as BB and fossil fuel combustions (Girach et al., 2014). BB should be major source for CO in the grain-producing areas (Huang et al., 2012; Ding et al., 2013).As mentioned in section 3.2.1, the peak CO level was also observed in Anhui and the west of Jiangsu, which was characterized by agriculture emissions (EP-6 and EP-7). However, the sources of CO in the northern China should further study in the future. The high levels of SO_2 was mainly observed in the east in Anhui and stretched to the Shanghai area (Figure 2c), suggesting high-sulfur fossil fuel were still widely utilized over the MLYP region. Whereas, SO_2 levels in Nanjing urban areas were measured at the background pollution levels. In general, NO_2 was regarded as a tracer for the local emission source, due to short lifetime in the atmosphere (Geng et al., 2009; Xu et al., 2011). NOx emissions mainly originated from vehicle and power plant (Fu et al., 2013). One can see that the NO_2 emission was characterized by strong local sources in north China and the YRD region (Figure 2d), which are in good agreement with the previous reports (Lin, 2011; Zhao et al., 2013a).

3.3 Chemical composition of fine particles during YRC and comparisons with other published data

The concentrations and mass fractions of the major ions and levoglucosan in $PM_{2.5}$ are shown in Figure 3. The water-soluble ions constitute one of the dominant components in atmospheric aerosol and determine the aerosol acidity (Kerminen et al., 2001), accounting for 37.43% and 40.15% in $PM_{2.5}$ and $PM_{1.0}$ during YRC, respectively. To access the data quality, ion balance gained by the major anions (SO_4^{2-}, NO_3^-, and Cl^-) and cations (Na^+, NH_4^+, K^+, Ca^{2+}, and Mg^{2+}) was calculated in this cruise. Both cations and anions are in the units of equivalent concentration (μ eq m^{-3}). There is a good correlation ($R^2 > 0.99$ and $R^2 > 0.98$, $P < 0.01$) between cation and anions (equivalent concentration) in $PM_{1.0}$ and $PM_{2.5}$, respectively, implying a high quality of data and same source of major ions in this cruise (Figure S5a) (Boreddy and Kawamura., 2015). Additionally, the relationship between NH_4^+ and Ca^{2+} vs SO_4^{2-} and NO_3^- was further investigated. As plotted in Figure S5b, the slopes of linear regression lines for [NH_4^++Ca^{2+}] vs [SO_4^{2-}+NO_3^-] in $PM_{2.5}$ and $PM_{1.0}$ were 1.171 and 1.154, respectively, suggesting that the alkaline substance in aerosol could completely neutralize SO_4^{2-} and NO_3^- during YRC.

For the ionic concentration, the most abundant species of $PM_{2.5}$ was SO_4^{2-} with a mean of 15.21 ± 6.69 μg m^{-3}, followed by NO_3^- (13.76 ± 4.99 μg m^{-3}), NH_4^+ (9.38 ± 4.35 μg m^{-3}), Ca^{2+} (2.23 ± 1.24 μg m^{-3}),

Cl$^-$ (1.94 ± 0.92 μg m^{-3}), Na$^+$ (1.29 ± 0.48 μg m^{-3}), K$^+$ (0.63 ± 0.22 μg m^{-3}), and Mg^{2+} (0.22 ± 0.07 μg m^{-3}) (Figure S6a). The mass concentration of SNA accounted for 85.89% of the total water-soluble ions in PM$_{2.5}$. Comparing with the previous reports (Figure 4), the SNA concentrations were much lower than those collected in the western and northern polluted cities in winter, including Beijing (38.90, 22.70, and 22.4 μg m^{-3}, respectively) (Wang et al., 2015a), Xi'an (39.7, 21.43, and 12.50 μg m^{-3}, respectively) (Xu et al., 2016a), Wuhan (29.80, 29.80, and 16.80 μg m^{-3}, respectively) (Zhang et al., 2015) and Chengdu (31.80, 15.5, and 15.5 μg m^{-3}, respectively) (Tao et al., 2014a). However, the concentrations of SNA were higher than those collected in marine boundary layer, such as East China sea (29.80, 29.80, and 16.80 μg m^{-3}, respectively) (Nakamura et al., 2005), Northern South China Sea (7.80, 0.24, and 2.1 μg m^{-3}, respectively) (Zhang et al., 2007), South China sea (7.99, 0.08, and 1.083 μg m^{-3}, respectively) (Hsu et al., 2007), Taiwan Strait (5.20, 3.13, and 1.50 μg m^{-3}, respectively) (Li et al., 2016), and Tuoji island in Bohai Rim (8.90, 5.80, and 1.40 μg m^{-3}, respectively) (Zhang et al., 2014). The SNA levels in the YRC were close to Shanghai in winter (11.7, 13.33, and 8.11 μg m^{-3}, respectively) (Zhou et al., 2016). The mass ratio of NO$_3^-$/SO$_4^{2-}$ was regarded as a marker to distinguish mobile source *vs.* stationary source (Huang et al., 2013). The ratio of NO$_3^-$/SO$_4^{2-}$ in this campaign was also close to that of Shanghai, and lower than that in other cities (Figure 4), indicating that mobile source emissions (traffic) contributed the most to fine particles. Besides, the mass concentration of SO$_4^{2-}$ definitely exceed the level of NO$_3^-$ in the marine boundary layer (Figure 4), indicating that marine source was another important source for SO$_4^{2-}$ (Calhoun et al., 1991). The average concentration of Ca^{2+}(2.23 μg m^{-3}) in this cruise was the highest among all locations and cruises (Figure 4), followed by Chengdu (2.10 μg m^{-3}), Wuhan (1.90 μg m^{-3}), and Xi'an (1.33 μg m^{-3}). As shown in Figure 4, Ca^{2+} also presented the higher concentration in the cities, and decreased from inland to coastal regions, indicating that Ca^{2+} was mainly from terrace crustal (Xiao et al., 2017). However, the concentrations of K$^+$ and Mg^{2+} for YRC were lower than those in the most samples among all location (Figure 4). K$^+$ may originate from BB, sea salt, and crustal dust. The average Cl$^-$ concentration during YRC was also lower than those in most cities (Figure 4). However, Na$^+$ level in this cruise was higher than the most reported values (Figure 4). The poor correlation between Na$^+$ and Cl$^-$ also indicated that two ions may have the different sources during YRC. Besides, the ratio of Cl$^-$/Na$^+$ among all location (Figure 4) were much higher than 1.17 (ratio of seawater), suggesting that anthropogenic sources, including BB and coal combustion, contributed the excessive Cl$^-$ in China cities (Li et al., 2015a; Zhang et al., 2013). The concentration of levoglucosan, a BB tracer, ranged from 0.015-

0.18 µg m^{-3} with a mean value of 0.075 ± 0.047 µg m^{-3}, much higher than the average concentration of

0.0394 µg m^{-3} in Lin'an (30.3°N, 119.73°E) (a rural site in the YRD region) (Liang et al., 2017),

indicating that BB was also a major contributor to PM$_{2.5}$ during YRC.

17 elements of PM$_{1.0}$ and PM$_{2.5}$ were measured, and the average concentrations are summarized in

Table 3. For comparison, the data reported previously in the megacities (in winter) and the cruises are

also outlined in Table 4. Ca show the highest concentration among all elements (Table 3) at all locations

(Table 4), and shared 2.16% on average in PM$_{2.5}$, partly due to cold front with floating dust in this

campaign. The secondary highest concentration among all elements was Fe (Table 3). This concentration

(1.64 µg m^{-3}) in the campaign was higher than those at many urban sites, such as Beijing (1.55 µg m^{-3})

(Zhao et al., 2013c), Shanghai (0.56 µg m^{-3}) (Huang et al., 2012b), and Guangzhou (0.16 µg m^{-3}) (Lai et

al., 2016), probably due to numerous steel industries/shipyards densely distributed on both banks of the

Yangtze River. Other elements decreased from K (865.88 ng m^{-3}) to Tl (0.32 ng m^{-3}). Pb and Zn

contributed the highest levels among heavy metals of PM$_{2.5}$. Except for inland cities, such as Beijing

(Zhao et al., 2013c), Wuhan (Zhang et al., 2015), and Chengdu (Tao et al., 2014a), the average

concentrations of Pb and Zn along the YRC were much higher than those in the other regions and cruises

(Table 4). Both Pb and Zn could originate from coal combustion and/or mineral industry, which were

related to energy structure and industrial layout over the MLYR region (Zhao et al., 2013c; Zhang et al.,

2015; Tao et al., 2014a; Zhao et al., 2015).

The enrichment factors (EFs) were applied to distinguish crustal elements from the anthropogenic

sources. The formula to evaluate EFs was:

$$EF_i = (X_i/X_R)_{\text{aerosol}} / (X'_i/X'_R)_{\text{crust}} \quad (3)$$

of which EF$_i$ is the enrichment factor of element i; X$_i$ and X$_R$ are the concentrations of element i and

reference element of R in aerosol, respectively; X'$_i$ and X'$_R$ are the background content of elements in

the MLYR soil (Wei et al., 1991). Al was determined to originate from soil. Hence, it was selected as

the reference element for the calculation. The elements of EFs < 10 included: Al, K, Mg, and Na, all of

which were regarded from crustal or re-suspension local soil. The species with higher EFs (10 < EFs <

100) were thought to be the mixture of the crustal and anthropogenic sources, including Cr, Cu, Co, Ni,

and V. Trace elements of EFs > 100, including Ca, Zn, Se, Pb, As, Mo, Fe, and Cd, were attributed to

anthropogenic sources. To further explore sources of trace elements and potential geographical

distributions, PCA was used to classify the main source of trace elements of $PM_{2.5}$ using the rotate

component matrix and PSCF for individual element was performed to infer the potential source and/or

pathway regions. As shown in Figure 5a, trace elements were classified into four categories (PCA), which

could explain 86.73% of the variance, indicating that the major sources of elements of $PM_{2.5}$ could be

considered and explained. More specifically, the first component (component 1) could account for 38.48%

of the variance, which was derived from coal combustion, including the high loadings of Cd, As, Pb, Tl,

and Se. Particularly, Se was generally considered as a tracer for coal combustion, due to its formation in

the high-temperature environment. Se produced by the rapid gas-to-particle conversion could undergo

long-range transport (Nriagu, 1989; Wen and Carignan, 2007). As shown in Figure S6b, a significant

correlation ($R^2 = 0.71$, $P < 0.01$) between SO_4^{2-} and Se also confirmed coal combustion. Furthermore, As

and Pb mainly originated from coal combustion after phasing out of leaded gasoline in China since 1997

(Xu et al., 2012), both of which had significantly correlations with Se. The component 2 with a variation

of 25.45%, contributed by the high loading of Al, Mg, Ca, and K, all of which obviously represented the

crustal or soil elements, and showed the low EFs values (EFs< 10, except Ca). Component 3, accounting

for 15.14% of the variation, was considered as the primary source of V, Co, and Ni. Both V and Ni were

usually regarded as a tracer of heavy oil combustion (Zhao et al., 2013b; Becagli et al., 2017). The fourth

component (component 4) showed the high loadings of Mn, Co, Zn, and Fe, all of which could explain

7.33% of the variance. Fe exhibited the high EFs value, indicating that these may originate from

anthropogenic sources. Anthropogenic Fe was usually deemed to originate from steel factory and/or

shipyard, both of which were densely distributed along the Yangtze River (Fu et al., 2014). Their

chemical processes and potential source contributions would be detailed in section 3.4.

3.4 Regional difference in formation mechanism of aerosol pollution and potential source contributions of element in $PM_{2.5}$ over the MLYR region

3.4.1 Secondary component pollution related to coal combustion in central China

As illustrated in Figure 3, the mass concentrations of SNA with an average of 38.35 ± 15.17 μg/m³

increased dramatically from coastal to inland cities and exhibited the highest level (#6, 79.06 μg/m³) in

Wuhan region (EP-4), accounting for nearly 50% of the local $PM_{2.5}$ mass loading. As mentioned above,

SO_2 and NO_x also presented the high concentration in this region. Furthermore, Wuhan and the

surrounding regions were controlled by a low-pressure system with the low wind speed and high RH

conditions (Figure S3), of which have been verified to cause haze episode (Zhao et al., 2013d; Quan et al., 2011; Wang et al., 2010). In addition, the ratio of NO_3^-/SO_4^{2-} in Wuhan area was close to the values of cities in northern China (relative low) (Figure 4), suggesting that the stationary sources (such as: coal-fired power station or stove emission) dominated in this region. Heavy clouds and high humidity in central China suggested aqueous phase transformation processes were probable the main reaction path of SO_4^{2-} from SO_2 (Wang et al., 2016; Zhao et al., 2013d). Besides, the mass fractions of SNA in $PM_{2.5}$ also peaked in the rural region (EP-2 and EP-6), which was in accord with the low ratio of T/B in these regions, suggesting that aerosol particles in the rural region were well aged.

Meanwhile, trace elements for coal combustion (component 1) had also the high concentration in EP-4 and EP-5 (Figure 5b) when the ship anchored in Wuhan and traveled through the Jiujiang area. As illustrated in Figure 6a-d, As, Cd, Pb, and Se showed the similar source distribution. The higher PSCF values in Hubei, Hunan, and Jiangxi provinces coincided well with the uneven regional distribution of the residential coal consumption (Figure S7) in central China, suggesting coal-related PM pollution was quite serious in this region during this cruise. The peak mass fraction of Cl^- and SO_4^{2-} in $PM_{2.5}$ in Wuhan was also confirmed this result Thus, it's concluded that coal combustion contributed significantly to serious pollution with the high SNA loading in Wuhan and the surrounding regions during sampling.

3.4.2 Mineral Dust in YRD region

Contrary to SNA distribution, the concentration of Ca^{2+} along this cruise increased from the mainland to the costal of East China Sea (Figure 3). The peak concentration of crustal elements (component 2) and Ca^{2+} mass fraction of $PM_{2.5}$ occurred in EP-7 when a cold front arrived and associated with northeast winds, accompanying with floating dust (Figure 3 and Figure 5b).In the Meantime, dust episode was verified by the MODIS true-color image on 2 and 3 December (Figure S4), further confirmed by a drastic decrease of RH with the prevailing northwest wind (Table 2 and Figure S3). As shown in Figure 6e-h, the YRD region and the Loess Plateau with the highest PSCF values were identified as the important source regions and/or pathways for crustal elements of Al, K, Mg and Ca. Meanwhile, the central China also showed the distribution of K and Mg, for which the coal combustion in this region could be primarily responsible. Furthermore, Ca showed the high EFs (EFs > 100), suggesting that the crustal element may not derive from natural source, but from anthropogenic re-suspension of road and/or construction activities along the Yangtze River. To further evaluate the impact of anthropogenic Ca, the equation below was applied:

$$Ca_{\text{anthropogenic}} = Ca_{\text{total}} - Al_{\text{total}} \times (Ca/Al)_{\text{crust}} \quad (4)$$

$(Ca/Al)_{\text{crust}}$ is the ratio of Ca to Al in the crust, and its value is 0.5. According to this method, the average $Ca_{\text{anthropogenic}}$ concentration was 2.15 μg m^{-3}, and the peak level reached to 3.42 μg m^{-3} on December 3. IF all of $Ca_{\text{anthropogenic}}$ in the samples of other cities and cruises (Table 4) were calculated according to the same method, its level in this cruise was much higher than those in other samples, suggesting that anthropogenic dust was dominated and distributed in the YRD region during the period.

Resembling Ca^{2+} distribution pattern, the maximum concentration and mass fraction of Na^+ and K^+ in $PM_{2.5}$ were also measured during EP-7. Significantly correlation between Ca^{2+} and K^+ suggested that dust could be the major source of K^+ in $PM_{2.5}$ sampled during YRC (Figure 3). In general, it's well known that dust particles with the high alkalinity could firstly neutralize SO_4^{2-} and NO_3^- in aerosol particles, then atmospheric ammonia was absorbed. The concentrations and mass fractions of SNA in $PM_{2.5}$ slightly increased at the end of the cruise (EP-7 and EP-8) (Figure 3) since carbonate in aerosol could enhance the uptake of acidic gases on particles (Huang et al., 2010). In the meanwhile, the increasing mass ratio of NO_3^-/SO_4^{2-} in EP-7 and EP-8 was attributed to two main reasons (Figure 3). The mobile sources (such as: vehicle emissions) increased and released a huge amount of NO_x when the vessel was close to the megacity (Huang et al., 2013). Furthermore, NO_2 could transform into NO_3^- via the heterogeneous process on dust aerosol surface (Nie et al., 2012).

3.4.3 Heavy metals in mega-city

Heavy metals have toxic effects on plants, animals, and human beings. However, there is no uniform stander concentration for control indicator (Sharma and Agrawal, 2005). The trace elements (component 3 and component 4), with highly EFs ranging from 24 to 1213, were considered to mainly come from heavy oil and industry, respectively. The high concentrations of V and Ni were observed when the ship berthed in the Waigaoqiao port berthing region of Shanghai (EP-8) (Figure 5b), where some field observations have also identified that heavy oil combustion exert a significant impact on the local air quality (Zhao et al., 2013b; Fu et al., 2014; Ding et al., 2017; Liu et al., 2017). It's also reported that the transition metals of Ni and V were greatly enriched in smaller particles with a diameter of < 1.0 μm (Jang et al., 2007). Fine particle Ni (Figure 6i) had almost same spatial distribution with Cr (Figure 6j), that Shanghai, Jiangsu, and the east of Anhui were identified as the major potential source regions and/or pathways, owing to ship emissions, nonferrous metal mining, and smelting industries. The Mongolian

plateau also was also the source region, indicating that nature dust may be another possible source for Cr and Ni. However, the high PSCF values of fine particle V were only derived from the YRD region and Mongolian plateau (Figure 6j). It's partly that V was considered to originate from heavy oil combustion, while Ni and Cr probably has other sources (Table S1) (Zhao et al., 2013b).

The temporal variations of component 4 peaked nearly in Wuhan and Shanghai (EP-4, EP-7, and EP-8) (Figure 5b) where China Baowu steel industry, and numerous shipyards were located in those regions (Ivošević et al., 2016). Fine particle Fe, Co, Mn, and Zn displayed similar regional distribution (Figure 6l-o), and the high PSCF levels were observed in the YRD region, indicating that steel industries and/or shipyards were densely distributed in East of Anhui, Jiangsu and Shanghai. Besides, the high PSCF value for Zn (Figure 6l) was also exhibited high value in Hubei, Henan, and Shanxi province, probably due to the influence of coal combustion and nonferrous metal smelting activities in these regions (Li et al., 2015b). Overall, it should be noted that anthropogenic sources in mega-cities (WNS) were dominant origins for trace elements in fine particles collected along this cruise.

3.4.4 Biomass burning in rural region

Numerous studies also have confirmed that levoglucosan mostly originate from BB (Liang et al., 2017; Ding et al., 2013b; Wan et al., 2017; Wang et al., 2014). The distribution of lev is irregular parabolic from inland to coastal areas in Figure 3. The maximum value of lev (0.18 μg m^{-3}) was observed in the rural of Anhui province (EP-6), while its level in YRD region (EP-8) was at very low levels. The elevated levels of CO and low-concentrations of SO_2 and NO_X also confirmed BB in EP6 and EP7 (Table 2). However, fire points couldn't be apparently observed in the satellite-detected fire maps (http://firefly.geog.umd.edu/firemap/), due to heavy cloud cover on 27 November and 1 December. During the whole observation periods, there was only one sample (#12, Figure S8) collected during BB event. It was verified by MODIS fire points, due to a cold front blowing heavy clouds away (Figure S4). The slightly higher lev concentration was observed in the night that was attributed to the lower boundary layer at night and BB for heating and cooking in the rural regions.

The levoglucosan concentration and ratio of OC to lev (OC/lev) were also widely applied to estimate the contribution of BB to OC in PM$_{2.5}$. An empirical model was utilized as proposed by Wan et al. (2017):

$$OC_{BB} = \left(\frac{[lev]}{[OC]}\right)_{ambient} \Big/ \left(\frac{[lev]}{[OC]}\right)_{BB} \quad (5)$$

The differences of the (lev/OC) $_{BB}$ ratio among different biomass fuels and combustion conditions were taken into account. So, the average (lev/OC)$_{BB}$ ratio of 8.14 % was selected to calculate the contribution of BB to OC (Wan et al., 2017). Figure S9 presents the variation of lev/OC ratio along the Yangtze River. The ratio of lev/OC during this cruise ranged from 0.03 % to 0.91 % with an average of 0.35 ± 0.24 %, which was comparable to that of Lin'an in YRD region (Liang et al., 2017). However, the ratio of lev/OC during YRC was near an order of magnitude of lower than its value in New Delhi (3.1 ± 0.8 %) (Li et al., 2014) and Lumbini (3.34 ± 2.53 %) in the northern edge of Indo-Gangetic Plain (Wan et al., 2017), where BB play an important role on air quality. Figure S9 also shows the time serious of contribution of BB-OC to OC. The average contribution of BB-OC/OC was 4.26 ± 2.89 %, while the mean mass fraction of OC to PM$_{2.5}$ was slightly higher than 20%. The peak contribution of OC deriving from BB to total OC of PM$_{2.5}$ nearly accounted for 11% in EP-6, which was approached that of the Pearl River region sites (13%) (Ho et al., 2014). Here, it's emphasized that our method based on empirical formula and value is just rough estimation. Hence, the radiocarbon measurement (^{14}C) of carbonaceous aerosol and air quality model simulation should need to confirm this result in the future.

3.5 Ship emission

3.5.1 Primary of ship emission

Over the past few decades, China's rapid economic development leads to the increasingly busy shipping transportation in the Yangtze River. However, there is lack of data related to ship emission along the stream of Yangtze River, especially in inland area. The ratio of V to Ni was used to judge whether ship emission could influence air quality (Isakson et al., 2001). The average ratio of V/Ni in the cruise is 1.27, which was in good agreement with the previous studies (Pandolfi et al., 2011; Zhang et al., 2014). Emission factors of heavy metals from different types of fuel oil were also analyzed in our group (Table S1). Only heavy oil contained V, while the V levels emitted from other diesel and petrol were under the detector limits. In this study, only V was regarded as the tracer for heavy oil combustion. However, it was still difficult to distinguish V from refinery and ship emission. Hence, the high-resolution back-trajectory and high-resolution of the ship position from the AIS data were applied to investigate ship plume during this cruise. As plotted in Figure 7, the numbers of the ship from AIS were closely related to the V concentrations. From the inland region to the East China Sea at Shanghai, the concentration of V of PM$_{2.5}$ generally increased, and reached the highest level of 0.06 μg m^{-3} on 4 December when the

vessel berthed in the anchorage of the Yangtze River estuary. Meanwhile, air masses in this evening originated from the port and anchorage (Figure S10). Hence, V of $PM_{2.5}$ sampled in the port of Shanghai could be probably attributable to ship emissions, especially from oceangoing vessels.

The contribution of primary ship emissions to $PM_{2.5}$ could be calculated by the equation developed by Agrawal et al. (2009):

$$PM_a = <a> \times <r> \times V_a / <F_{V,HFO}> \quad (6)$$

where PM_a represents the primary $PM_{2.5}$ concentration estimated (μg m^{-3}); $<a>$ is a coefficient of the fraction of V from ship emissions in fine particles in China (0.85), $<r>$ is average ratio of $PM_{2.5}$ to normalized V emitted (ppm); V_a represents the V amount of the samples (μg m^{-3}) during YRC, and is the V content of heavy oil on average from the vessels (ppm). The value of $<r>$ was set as 8205.8 ppm as Agrawal et al. (2009) reported. The value of $<F_{V,HFO}>$ was set as 65.3 ppm, of which represents of the average V contents (Zhao et al., 2013b). The average concentration of the primary ship emission was 1.01 ± 1.41 μg m^{-3}, ranging from 0.02 to 6.27 μg m^{-3}, which is higher than that at Tuoji Island (0.65 μg m^{-3}) (Zhang et al., 2014). The peak level of primary ship emission was observed in the Shanghai harbor.

3.5.2 Ship emission contribution to SO_4^{2-}, NO_3^-, and OC

To in-depth characterize the contribution of the ship emissions to secondary fine particles, a lower limit of the SO_4^{2-}/V, NO_3^-/V, EC/V, and OC/V ratios (equal to the average minus one standard deviation) was applied to estimate the particulate from heavy oil combustion in the course of the Yangtze River (Becagli et al., 2017). As presented in Figure S11a-b, the mass ratio of SO_4^{2-}/V and NO_3^-/V decreased rapidly with increasing V concentration. According to ship traffic numbers, weather condition, and the emission factors of different type oils (Table S1), the samples with V > 15 ng m^{-3} were mainly considered to come from ship emissions.

The limit ratio of SO_4^{2-}/V, NO_3^-/V and OC/V, and the estimation of ship emissions contributions to SO_4^{2-}, NO_3^-, OC, and $PM_{2.5}$ are summarized in Table S2 in supporting information. The minimum ratio of NO_3^-/V in this cruise was nearly twice greater than the limit ratio for SO_4^{2-}/V, which was contrary to the previous results with higher SO_4^{2-} from ship emissions observed in summer on the island of Lampedusa (35.5°N, 12.6°E) in the central Mediterranean. In general, SO_4^{2-} and NO_3^- in aerosol were mainly formed

through gas precursors of SO_2 and NO_X, respectively, both of which were completely different for lift-time and chemical processes in the atmosphere. High UV radiation and humidity could accurate the reaction rate of SO_2 to SO_4^{2-} (Zhou et al., 2016). However, NO_3^- was in gas-aerosol equilibrium with gaseous HNO_3 (g). Low temperature and humidity would shift the gas-aerosol equilibrium to the particle phase (NO_3^-) (Matthias et al., 2010; Wang et al., 2016). One reason for this discrepancy was probably meteorological and photochemical conditions, which leaded to lower sulfur conversion rate, and particulate NO_3^- domination in the low temperature and moisture in winter during this cruise (Table 2). On the other hand, NO_3^- may have other sources in Shanghai port, whereas Lampedusa was a remote site (Becagli et al., 2017). The average estimated concentration of minimum SO_4^{2-} derived from ship emission was 1.38 μg m^{-3} during YRC, which was similar to the value (1.35 μg m^{-3}) measured in the Mediterranean (Becagli et al., 2017; Becagli, 2012).

EC and OC were also estimated by the same methods for SO_4^{2-} and NO_3^-, and the lower limit for OC/V and EC/V ratio are also presented in Figure S11c-d. Besides, significant correlation between V and EC (R^2 = 0.71, P < 0.01) suggested that V and EC have same sources (Agrawal et al., 2009). In this cruise, organic matter (OM) of $PM_{2.5}$ were estimated from OC by multiplying a conversion factor of 1.4, due to typical fresh emission and weak light in winter (Becagli et al., 2017). The estimated lower limit for average of ship emissions was 7.65 μg m^{-3}, nearly occupying 6.41% of $PM_{2.5}$ during YRC. The peak ship contribution could reach to 36.04% of total $PM_{2.5}$ when the vessel berthed in the Waigaoqiao port of Shanghai, which was slight above the value (20-30%) estimated by Liu et al. (2017) during ship-plume-influenced periods. It should be noted that the ship emission decreased from Shanghai port to the inland area. One reason for this was correspond to the density of ship in the Yangtze River channel. On the other hand, fuel oils were completely different between the ship travelling in inland waterway and the oceangoing vessel. In general, light diesel with low EFs of heavy metals (such as: V, Ni) was widely used by the ships on river, whereas heavy oil showing high content of V and Ni were widely burned onboard marine vessels as fuel (Table S1). Oceangoing ship emissions were probably the major air pollution sources in the Shanghai port. Hence, it is urgent to establish emission control areas (ECAs) in Shanghai ports. However, it is worth noting that our estimation based on empirical values was also limited by meteorological conditions and sample numbers. Hence, long-term observation and high resolutions model simulation of ship emissions should be strengthened as part of control of air quality along the Yangtze River, especially in Shanghai harbor cluster.

4 Conclusion

In order to better characterize air quality over the region of MLYR, an intensive atmospheric observation was conducted during YRC. A shipboard measurement was conducted to measure and analysis an suite of air pollutants (trace gases and fine particles) in this region. The average concentrations of $PM_{1.0}$ and $PM_{2.5}$ were 96.69 ± 22.18 μg m^{-3} and 119.29 ± 33.67 μg m^{-3} during the cruise, respectively. The most abundant ionic species in $PM_{2.5}$ was SO_4^{2-} with an average concentration of 15.21 ± 6.69 μg/m^3, followed by NO_3^- (13.76 ± 4.99μg/m^3), NH_4^+ (9.38 ± 4.35μg/m^3), Ca^{2+} (2.23 ± 1.24μg/m^3), Cl^- (1.94 ± 0.92 μg m^{-3}), Na^+ (1.29 ± 0.48 μg m^{-3}), K^+ (0.63 ± 0.22 μg m^{-3}), and Mg^{2+} (0.22 ± 0.07 μg m^{-3}), respectively. Combined with satellite data, back trajectory, principal component analysis (PCA), and potential source contribution function (PSCF), major chemical composition of $PM_{2.5}$ manifested greatly geographical differences and diverse anthropogenic emission sources from coastal to inland regions. Wuhan suffered secondary aerosol pollution with SNA accounting for nearly 50% of $PM_{2.5}$. The significant correlation between Se and SO_4^{2-} revealed that the stationary emissions may play an important role in SNA formation. The concentrations of levoglucosan of $PM_{2.5}$ and CO column levels from the satellite data significantly enhanced in the rural areas (Anhui and Jiangxi), indicating that BB from the both shores of the Yangtze River may make remarkable contribution to air pollution in rural area during YRC. Further, the crustal elements of Al and Ca presented the high levels in the YRD regions and the high value of enrichment factors (EFs) of Ca (EFs > 100) coupling with the PSCF results suggested the crustal elements may derive from re-suspension of dust from road and/or construction activity along the banks of the Yangtze River. Ship emissions displayed a significant effect on air pollution, and could contribute to more than 36% of $PM_{2.5}$ in the ports of Shanghai. As far as we know, it's the first comprehensive observation of air quality over the MLYR region using a vessel mobile platform. The results herein suggested that the differentiated control measures in accordance with local pollution characteristics should be taken to tackle air pollution.

Competing interests

The authors claim that they have no competing interests.

Acknowledgements

This work was supported by the Ministry of Science and Technology of China (No. 2016YFC0202700, 2014BAC22B00), the National Natural Science Foundation of China (No. 91743202, 21527814) and Marie Skłodowska-Curie Actions (690958-MARSU-RISE-2015).

582 References:

583 Ackerman, A. S., Kirkpatrick, M. P., Stevens, D. E., and Toon, O. B.: The impact of humidity above

584 stratiform clouds on indirect aerosol climate forcing, Nature, 432, 1014, 2004.

585 Agrawal, H., Eden, R., Zhang, X., Fine, P. M., Katzenstein, A., Miller, J. W., Ospital, J., and Teffera, S.:

586 Primary particulate matter from ocean-going engines in the Southern California Air Basin, Environ. Sci.

587 Technol., 43, 5398-5402, 2009.

588 An, J., Wang, H., Shen, L., Zhu, B., Zou, J., Gao, J., and Kang, H.: Characteristics of new particle

589 formation events in Nanjing, China: Effect of water-soluble ions, Atmos. Environ., 108, 32-40,

590 10.1016/j.atmosenv.2015.01.038, 2015.

591 Baltrenas, P., Baltrenaite, E., Sereviciene, V., and Pereira, P.: Atmospheric BTEX concentrations in the

592 vicinity of the crude oil refinery of the Baltic region, Environ. Monit. Assess., 182, 115-127, 2011.

593 Becagli, S., Anello, F., Bommarito, C., Cassola, F., Calzolai, G., Di Iorio, T., di Sarra, A., Gómez-Amo,

594 J.-L., Lucarelli, F., Marconi, M., Meloni, D., Monteleone, F., Nava, S., Pace, G., Severi, M., Sferlazzo,

595 D. M., Traversi, R., and Udisti, R.: Constraining the ship contribution to the aerosol of the central

596 Mediterranean, Atmos. Chem. Phys., 17, 2067-2084, 10.5194/acp-17-2067-2017, 2017.

597 Becagli, S. S., D. M.Pace, G.di Sarra, A.Bommarito, C.Calzolai, G.Ghedini, C.Lucarelli, F.Meloni,

598 D.Monteleone, F.Severi, M.Traversi, R.Udisti, R.: Evidence for heavy fuel oil combustion aerosols from

599 chemical analyses at the island of Lampedusa: a possible large role of ships emissions in the

600 Mediterranean, Atmos. Chem. Phys., 12, 3479-3492, 10.5194/acp-12-3479-2012, 2012.

601 Boreddy, S. K. R., and Kawamura, K.: A 12-year observation of water-soluble ions in TSP aerosols

602 collected at a remote marine location in the western North Pacific: an outflow region of Asian dust,

603 Atmos. Chem. Phys., 15, 6437-6453, 10.5194/acp-15-6437-2015, 2015.

604 Calhoun, J. A., Bates, T. S., and Charlson, R. J.: Sulfur isotope measurements of submicrometer sulfate

605 aerosol particles over the Pacific Ocean, Geophys. Res. Lett., 18, 1877-1880, 10.1029/91gl02304, 1991.

606 Chameides, W. L., Yu, H., Liu, S. C., Bergin, M., Zhou, X., Mearns, L., Wang, G., Kiang, C. S., Saylor,

607 R. D., and Luo, C.: Case study of the effects of atmospheric aerosols and regional haze on agriculture:

608 an opportunity to enhance crop yields in China through emission controls?, Proc. Nat. Acad. Sci. U.S.A.,

609 96, 13626-13633, 1999.

610 Cheng, Z., Wang, S., Fu, X., Watson, J. G., Jiang, J., Fu, Q., Chen, C., Xu, B., Yu, J., and Chow, J. C.:

611 Impact of biomass burning on haze pollution in the Yangtze River delta, China: a case study in summer

2011, Atmos. Chem. Phys., 14, 4573-4585, 10.5194/acp-14-4573-2014, 2014.

Coggon, M. M., Sorooshian, A., Wang, Z., Metcalf, A. R., Frossard, A. A., Lin, J. J., Craven, J. S., Nenes, A., Jonsson, H. H., Russell, L. M., Flagan, R. C., and Seinfeld, J. H.: Ship impacts on the marine atmosphere: insights into the contribution of shipping emissions to the properties of marine aerosol and clouds, Atmos. Chem. Phys., 12, 8439-8458, 10.5194/acp-12-8439-2012, 2012.

Ding, A. J., Fu, C. B., Yang, X. Q., Sun, J. N., Petäjä, T., Kerminen, V. M., Wang, T., Xie, Y., Herrmann, E., and Zheng, L. F.: Intense atmospheric pollution modifies weather: a case of mixed biomass burning with fossil fuel combustion pollution in eastern China, Atmos. Chem. Phys., 13, 10545-10554, 10.5194/acp-13-10545-2013, 2013a.

Ding, X., Wang, X., Xie, Z., Zhang, Z., and Sun, L.: Impacts of Siberian biomass burning on organic aerosols over the North Pacific Ocean and the Arctic: primary and secondary organic tracers, Environ. Sci. Technol., 47, 3149-3157, 2013b.

Ding, X., Kong, L., Du, C., Zhanzakova, A., Wang, L., Fu, H., Chen, J., Yang, X., and Cheng, T.: Long-range and regional transported size-resolved atmospheric aerosols during summertime in urban Shanghai, Sci. Total Environ., 583, 334-343, 2017.

Draxler, R. R., and Hess, G. D.: An overview of the HYSPLIT_4 modelling system for trajectories, Aust. Meteorol. Mag., 47, 295-308, 1998.

Fan, Q., Zhang, Y., Ma, W., Ma, H., Feng, J., Yu, Q., Yang, X., Ng, S. K., Fu, Q., and Chen, L.: Spatial and Seasonal Dynamics of Ship Emissions over the Yangtze River Delta and East China Sea and Their Potential Environmental Influence, Environ. Sci. Technol., 50, 1322-1329, 2016.

Fu, H. B., Shang, G. F., Lin, J., Hu, Y. J., Hu, Q. Q., Guo, L., Zhang, Y. C., and Chen, J. M.: Fractional iron solubility of aerosol particles enhanced by biomass burning and ship emission in Shanghai, East China, Sci. Tot. Environ., 481, 377-391, 2014.

Fu, X., Wang, S., Zhao, B., Xing, J., Cheng, Z., Liu, H., and Hao, J.: Emission inventory of primary pollutants and chemical speciation in 2010 for the Yangtze River Delta region, China, Atmos. Environ., 70, 39-50, 2013.

Gaston, C. J., Quinn, P. K., Bates, T. S., Gilman, J. B., Bon, D. M., Kuster, W. C., and Prather, K. A.: The impact of shipping, agricultural, and urban emissions on single particle chemistry observed aboard the R/V Atlantis during CalNex, J. Geophys. Res. Atmos., 118, 5003-5017, 10.1002/jgrd.50427, 2013.

Geng, F., Zhang, Q., Tie, X., Huang, M., Ma, X., Deng, Z., Yu, Q., Quan, J., and Zhao, C.: Aircraft

642 measurements of O3, NOx, CO, VOCs, and SO2 in the Yangtze River Delta region, Atmos. Environ.,

643 43, 584-593, 2009.

644 Girach, I., Nair, V. S., Babu, S. S., and Nair, P. R.: Black carbon and carbon monoxide over Bay of

645 Bengal during W_ICARB: Source characteristics, Atmos. Environ., 94, 508-517, 2014.

646 Han, T., Qiao, L., Zhou, M., Qu, Y., Du, J., Liu, X., Lou, S., Chen, C., Wang, H., and Zhang, F.: Chemical

647 and optical properties of aerosols and their interrelationship in winter in the megacity Shanghai of China,

648 J. Environ. Sci., 27, 59-69, 2015.

649 Han, Y.-J., Holsen, T. M., Hopke, P. K., and Yi, S.-M.: Comparison between back-trajectory based

650 modeling and Lagrangian backward dispersion modeling for locating sources of reactive gaseous

651 mercury, Environ. Sci. Technol., 39, 1715-1723, 2005.

652 He, Q., Li, C., Geng, F., Yang, H., Li, P., Li, T., Liu, D., and Pei, Z.: Aerosol optical properties retrieved

653 from Sun photometer measurements over Shanghai, China, J. Geophys. Res. Atmos., 117, D16204,

654 10.1029/2011jd017220, 2012.

655 Ho, K. F., Engling, G., Sai Hang Ho, S., Huang, R., Lai, S., Cao, J., and Lee, S. C.: Seasonal variations

656 of anhydrosugars in PM2.5 in the Pearl River Delta Region, China, Tellus B: Chemical and Physical

657 Meteorology, 66, 22577, 10.3402/tellusb.v66.22577, 2014.

658 Hopke, P. K., Barrie, L. A., Li, S. M., Cheng, M. D., Li, C., and Xie, Y.: Possible sources and preferred

659 pathways for biogenic and non-sea-salt sulfur for the high Arctic, J. Geophys. Res. Atmos., 100, 16595-

660 16603, 10.1029/95JD01712, 1995.

661 Hsu, S.-C., Liu, S. C., Kao, S.-J., Jeng, W.-L., Huang, Y.-T., Tseng, C.-M., Tsai, F., Tu, J.-Y., and Yang,

662 Y.: Water-soluble species in the marine aerosol from the northern South China Sea: High chloride

663 depletion related to air pollution, J. Geophys. Res., 112, 10.1029/2007jd008844, 2007.

664 Huang, K., Zhuang, G., Lin, Y., Fu, J. S., Wang, Q., Liu, T., Zhang, R., Jiang, Y., Deng, C., and Fu, Q.:

665 Typical types and formation mechanisms of haze in an Eastern Asia megacity, Shanghai, Atmos. Chem.

666 Phys., 12, 105, 10.5194/acp-12-105-2012, 2012a.

667 Huang, K., Zhuang, G., Lin, Y., Wang, Q., Fu, J. S., Zhang, R., Li, J., Deng, C., and Fu, Q.: Impact of

668 anthropogenic emission on air quality over a megacity–revealed from an intensive atmospheric campaign

669 during the Chinese Spring Festival, Atmos. Chem. Phys., 12, 11631-11645, 10.5194/acp-12-11631-2012,

670 2012b.

671 Huang, K., Zhuang, G., Lin, Y., Wang, Q., Fu, J. S., Fu, Q., Liu, T., and Deng, C.: How to improve the

672   air quality over megacities in China: pollution characterization and source analysis in Shanghai before,

673   during, and after the 2010 World Expo, Atmos. Chem. Phys., 13, 5927-5942, 10.5194/acp-13-5927-2013,

674   2013.

675   Isakson, J., Persson, T. A., and Lindgren, E. S.: Identification and assessment of ship emissions and their

676   effects in the harbour of Göteborg, Sweden, Atmos. Environ., 35, 3659-3666, 2001.

677   Ivošević, T., Stelcer, E., Orlić, I., Bogdanović Radović, I., and Cohen, D.: Characterization and source

678   apportionment of fine particulate sources at Rijeka, Croatia from 2013 to 2015, Nucl. Instrum. Methods.

679   Phys. Res. B., 371, 376-380, 2016.

680   Jalkanen, J., Johansson, L., and Kukkonen, J.: A comprehensive inventory of ship traffic exhaust

681   emissions in the European sea areas in 2011, Atmos. Chem. Phys., 16, 71-84, 2015.

682   Jang, H. N., Lee, S. J. H., Hwang, K. W., Yoo, J. I., Sok, C. H., and Kim, S. H.: Formation of fine

683   particles enriched by V and Ni from heavy oil combustion: Anthropogenic sources and drop-tube furnace

684   experiments, Atmos. Environ., 41, 1053-1063, 2007.

685   Jones, A. D. L. A., Roberts, D. L., and Slingo, A.: A climate model study of indirect radiative forcing by

686   anthropogenic sulphate aerosols, Nature, 370, 450-453, 1994.

687   Kang, H., Zhu, B., Su, J., Wang, H., Zhang, Q., and Wang, F.: Analysis of a long-lasting haze episode in

688   Nanjing, China, Atmos. Res., 78-87, 2013a.

689   Kang, H., Zhu, B., Su, J., Wang, H., Zhang, Q., and Wang, F.: Analysis of a long-lasting haze episode in

690   Nanjing, China, Atmos. Res., 120-121, 78-87, 2013b.

691   Kerminen, V.-M., Hillamo, R., Teinilä, K., Pakkanen, T., Allegrini, I., and Sparapani, R.: Ion balances

692   of size-resolved tropospheric aerosol samples: implications for the acidity and atmospheric processing

693   of aerosols, Atmos. Environ., 35, 5255-5265, 2001.

694   Kong, S., Li, X., Li, L., Yin, Y., Chen, K., Yuan, L., Zhang, Y., Shan, Y., and Ji, Y.: Variation of

695   polycyclic aromatic hydrocarbons in atmospheric PM2.5 during winter haze period around 2014 Chinese

696   Spring Festival at Nanjing: Insights of source changes, air mass direction and firework particle injection,

697   Sci. Tot. Environ., 520, 59-72, 2015.

698   Lai, S., Zhao, Y., Ding, A., Zhang, Y., Song, T., Zheng, J., Ho, K. F., Lee, S.-c., and Zhong, L.:

699   Characterization of PM2.5 and the major chemical components during a 1-year campaign in rural

700   Guangzhou, Southern China, Atmos. Res., 167, 208-215, 2016.

701   Li, C., Ma, Z., Chen, J., Wang, X., Ye, X., Wang, L., Yang, X., Kan, H., Donaldson, D. J., and Mellouki,

A.: Evolution of biomass burning smoke particles in the dark, Atmos. Environ., 120, 244-252, 2015a.

Li, J., Wang, G., Aggarwal, S. G., Huang, Y., Ren, Y., Zhou, B., Singh, K., Gupta, P. K., Cao, J., and Zhang, R.: Comparison of abundances, compositions and sources of elements, inorganic ions and organic compounds in atmospheric aerosols from Xi'an and New Delhi, two megacities in China and India, Sci. Total Environ., 476-477, 485-495, 10.1016/j.scitotenv.2014.01.011, 2014.

Li, T.-C., Yuan, C.-S., Hung, C.-H., Lin, H.-Y., Huang, H.-C., and Lee, C.-L.: Chemical Characteristics of Marine Fine Aerosols over Sea and at Offshore Islands during Three Cruise Sampling Campaigns in the Taiwan Strait– Sea Salts and Anthropogenic Particles, Atmos. Chem. Phys. Discuss., 1-27, 10.5194/acp-2016-384, 2016.

Li, T., Wang, Y., Li, W. J., Chen, J. M., Wang, T., and Wang, W. X.: Concentrations and solubility of trace elements in fine particles at a mountain site, southern China: regional sources and cloud processing, Atmos. Chem. Phys., 15, 8987-9002, 10.5194/acp-15-8987-2015, 2015b.

Liang, L., Engling, G., Zhang, X., Sun, J., Zhang, Y., Xu, W., Liu, C., Zhang, G., Liu, X., and Ma, Q.: Chemical characteristics of PM2.5 during summer at a background site of the Yangtze River Delta in China, Atmos. Res., 198, 163-172, 2017.

Liao, T., Wang, S., Ai, J., Gui, K., Duan, B., Zhao, Q., Zhang, X., Jiang, W., and Sun, Y.: Heavy pollution episodes, transport pathways and potential sources of PM2.5 during the winter of 2013 in Chengdu (China), Sci. Total Environ., 584, 1056-1065, 2017.

Lin, J. T.: Satellite constraint for emissions of nitrogen oxides from anthropogenic, lightning and soil sources over East China on a high-resolution grid, Atmos. Chem. Phys., 11, 29807-29843, 10.5194/acp-12-2881-2012, 2011.

Liu, Z., Lu, X., Feng, J., Fan, Q., Zhang, Y., and Yang, X.: Influence of Ship Emissions on Urban Air Quality: A Comprehensive Study Using Highly Time-Resolved Online Measurements and Numerical Simulation in Shanghai, Environ. Sci. Technol., 51, 202-211, 2017.

Matthias, V., Bewersdorff, I., Aulinger, A., and Quante, M.: The contribution of ship emissions to air pollution in the North Sea regions, Environ. Pollut., 158, 2241-2250, 10.1016/j.envpol.2010.02.013, 2010.

Moldanová, J., Fridell, E., Popovicheva, O., Demirdjian, B., Tishkova, V., Faccinetto, A., and Focsa, C.: Characterisation of particulate matter and gaseous emissions from a large ship diesel engine, Atmos. Environ., 43, 2632-2641, 2009.

732   Nakamura, T., Matsumoto, K., and Uematsu, M.: Chemical characteristics of aerosols transported from

733   Asia to the East China Sea: an evaluation of anthropogenic combined nitrogen deposition in autumn,

734   Atmos. Environ., 39, 1749-1758, 2005.

735   Novakov, T., and Penner, J. E.: Large contribution of organic aerosols to cloud-condensation-nuclei

736   concentrations, Nature, 365, 823-826, 1993.

737   Nriagu, J. O.: A global assessment of natural sources of atmospheric trace metals, Nature, 338, 47-49,

738   1989.

739   Pandis, S. N., Capaldo, K., Corbett, J. J., Kasibhatla, P., and Fischbeck, P.: Effects of ship emissions on

740   sulphur cycling and radiative climate forcing over the ocean, Nature, 400, 743-746, 1999.

741   Pandolfi, M., Gonzalez-Castanedo, Y., Alastuey, A., Jd, D. L. R., Mantilla, E., As, D. L. C., Querol, X.,

742   Pey, J., Amato, F., and Moreno, T.: Source apportionment of PM10 and PM2.5 at multiple sites in the

743   strait of Gibraltar by PMF: impact of shipping emissions, Environ Sci Pollut Res, 18, 260-269, 2011.

744   Pöschl, U.: Atmospheric aerosols: composition, transformation, climate and health effects, Angew. Chem.

745   Int. Ed., 44, 7520-7540, 2005.

746   Quan, J., Zhang, Q., He, H., Liu, J., Huang, M., and Jin, H.: Analysis of the formation of fog and haze in

747   North China Plain (NCP), Atmos. Chem. Phys., 11, 8205-8214, 10.5194/acp-11-8205-2011, 2011.

748   Seaton, A., Godden, D., MacNee, W., and Donaldson, K.: Particulate air pollution and acute health

749   effects, The lancet, 345, 176-178, 1995.

750   Sharma, R. K., and Agrawal, M.: Biological effects of heavy metals: An overview, J. Environ. Biol., 26,

751   301, 2005.

752   Shen, G. F., Yuan, S. Y., Xie, Y. N., Xia, S. J., Li, L., Yao, Y. K., Qiao, Y. Z., Zhang, J., Zhao, Q. Y.,

753   and Ding, A. J.: Ambient levels and temporal variations of PM2.5 and PM10 at a residential site in the

754   mega-city, Nanjing, in the western Yangtze River Delta, China, Journal of Environmental Science and

755   Health, Part A, 49, 171-178, 2014.

756   Stier, P., Feichter, J., Kinne, S., Kloster, S., Vignati, E., Wilson, J., Ganzeveld, L., Tegen, I., Werner, M.,

757   and Balkanski, Y.: The aerosol-climate model CHAM5-HAM, Atmos. Chem. Phys., 5, 1125-1156,

758   10.5194/acp-5-1125-2005 2005.

759   Sun, X., Luo, X., Yan, C., Zhen, Z., Xu, J., Zhang, D., Suo, C., and Ding, Y.: Spatio-temporal

760   characteristics of air pollution in Nanjing during 2013 to 2016 under the pollution control and

761   meteorological factors, J. Environ. Earth., 8, 506-515, 2017.

Tao, J., Gao, J., Zhang, L., Zhang, R., Che, H., Zhang, Z., Lin, Z., Jing, J., Cao, J., and Hsu, S. C.: PM2.5 pollution in a megacity of southwest China: source apportionment and implication, Atmos. Chem. Phys., 14, 8679-8699, 10.5194/acp-14-8679-2014, 2014a.

Tao, Y., Yin, Z., Ye, X., Ma, Z., and Chen, J.: Size distribution of water-soluble inorganic ions in urban aerosols in Shanghai, Atmos. Pollut. Res., 5, 639-647, 2014b.

Wan, X., Kang, S., Li, Q., Rupakheti, D., Zhang, Q., Guo, J., Chen, P., Tripathee, L., Rupakheti, M., Panday, A. K., Wang, W., Kawamura, K., Gao, S., Wu, G., and Cong, Z.: Organic molecular tracers in the atmospheric aerosols from Lumbini, Nepal, in the northern Indo-Gangetic Plain: influence of biomass burning, Atmos. Chem. Phys., 17, 8867-8885, 10.5194/acp-17-8867-2017, 2017.

Wang, G., Zhang, R., Gomez, M. E., Yang, L., Levy Zamora, M., Hu, M., Lin, Y., Peng, J., Guo, S., Meng, J., Li, J., Cheng, C., Hu, T., Ren, Y., Wang, Y., Gao, J., Cao, J., An, Z., Zhou, W., Li, G., Wang, J., Tian, P., Marrero-Ortiz, W., Secrest, J., Du, Z., Zheng, J., Shang, D., Zeng, L., Shao, M., Wang, W., Huang, Y., Wang, Y., Zhu, Y., Li, Y., Hu, J., Pan, B., Cai, L., Cheng, Y., Ji, Y., Zhang, F., Rosenfeld, D., Liss, P. S., Duce, R. A., Kolb, C. E., and Molina, M. J.: Persistent sulfate formation from London Fog to Chinese haze, Proc. Natl. Acad. Sci. U.S.A, 113, 13630-13635, 2016.

Wang, H., Lou, S., Huang, C., Qiao, L., Tang, X., Chen, C., Zeng, L., Wang, Q., Zhou, M., and Lu, S.: Source Profiles of Volatile Organic Compounds from Biomass Burning in Yangtze River Delta, China, Aerosol. Air. Qual. Res., 14, 818–828, 2014.

Wang, H., Tian, M., Li, X., Chang, Q., Cao, J., Yang, F., Ma, Y., and He, K.: Chemical Composition and Light Extinction Contribution of PM2.5 in Urban Beijing for a 1-Year Period, Aerosol Air Qual. Res, 15, 2200-2211, 2015a.

Wang, H. L., Qiao, L. P., Lou, S. R., Zhou, M., Chen, J. M., Wang, Q., Tao, S. K., Chen, C. H., Huang, H. Y., Li, L., and Huang, C.: PM2.5 pollution episode and its contributors from 2011 to 2013 in urban Shanghai, China, Atmos. Environ., 123, 298-305, 2015b.

Wang, S., Yu, S., Yan, R., Zhang, Q., Li, P., Wang, L., Liu, W., and Zheng, X.: Characteristics and origins of air pollutants in Wuhan, China, based on observations and hybrid receptor models, J. Air Waste Manage. Assoc., 67, 739-753, 10.1080/10962247.2016.1240724, 2017.

Wang, T., Nie, W., Gao, J., Xue, L. K., Gao, X. M., Wang, X. F., Qiu, J., Poon, C. N., .Meinardi, S., Blake, D., Wang, S. L., Ding, A. J., Chai, F. H., Zhang, Q. Z., and Wang, W. X.: Air quality during the 2008 Beijing Olympics: secondary pollutants and regional impact, Atmos. Chem. Phys., 10, 7603-7615,

792   10.5194/acp-10-7603-2010, 2010.

793   Wang, X., Bi, X., Sheng, G., and Fu, J.: Hospital indoor PM10/PM2.5 and associated trace elements in

794   Guangzhou, China, Sci. Total Environ., 366, 124-135, 10.1016/j.scitotenv.2005.09.004, 2006.

795   Wang, X., Miao, Y., Zhang, Y., Li, Y., Wu, M., and Yu, G.: Primary sources and secondary formation

796   of organic aerosols in Beijing, China, Environ. Sci. Technol., 46, 9846-9853, 2012.

797   Wang, Y. Q., Zhang, X. Y., and Draxler, R. R.: TrajStat: GIS-based software that uses various trajectory

798   statistical analysis methods to identify potential sources from long-term air pollution measurement data,

799   Environ. Model. Software, 24, 938-939, 2009.

800   Wei, F., Chen, J., Wu, Y., and Zheng, C.: Study of the background contents of 61 elements of soils in

801   China, Environmental Science, 12, 12-19, 1991

802   Wen, H., and Carignan, J.: Reviews on atmospheric selenium: Emissions, speciation and fate, Atmos.

803   Environ., 41, 7151-7165, 2007.

804   Xiao, H., Xiao, H., Luo, L., Shen, C., Long, A., Chen, L., Long, Z., and Li, D.: Atmospheric aerosol

805   compositions over the South China Sea: temporal variability and source apportionment, Atmos. Chem.

806   Phys., 17, 3199-3214, 10.5194/acp-17-3199-2017, 2017.

807   Xu, H., Cao, J., Chow, J. C., Huang, R.-J., Shen, Z., Chen, L. A., Ho, K. F., and Watson, J. G.: Inter-

808   annual variability of wintertime PM2.5 chemical composition in Xi'an, China: Evidences of changing

809   source emissions, Sci. Tot. Environ., 545, 546-555, 2016a.

810   Xu, H. M., Cao, J. J., Ho, K. F., Ding, H., Han, Y. M., Wang, G. H., Chow, J. C., Watson, J. G., Khol,

811   S. D., Qiang, J., and Li, W. T.: Lead concentrations in fine particulate matter after the phasing out of

812   leaded gasoline in Xi'an, China, Atmos. Environ., 46, 217-224, 2012.

813   Xu, W. Y., Zhao, C. S., Ran, L., Deng, Z. Z., Liu, P. F., Ma, N., Lin, W. L., Xu, X. B., Yan, P., He, X.,

814   Yu, J., Liang, W. D., and Chen, L. L.: Characteristics of pollutants and their correlation to meteorological

815   conditions at a suburban site in the North China Plain, Atmos. Chem. Phys., 11, 4353-4369, 10.5194/acp-

816   11-4353-2011, 2011.

817   Xu, X., Zhao, T., Liu, F., Gong, S. L., Kristovich, D., Lu, C., Guo, Y., Cheng, X., Wang, Y., and Ding,

818   G.: Climate modulation of the Tibetan Plateau on haze in China, Atmos. Chem. Phys., 16, 1365-1375,

819   10.5194/acp-16-1365-2016, 2016b.

820   Zhan, J., Gao, Y., Li, W., Chen, L., Lin, H., and Lin, Q.: Effects of ship emissions on summertime

821   aerosols at Ny–Alesund in the Arctic, Atmos. Pollut. Res., 5, 500-510, 2014.

822 Zhang, F., Chen, Y., Tian, C., Wang, X., Huang, G., Fang, Y., and Zong, Z.: Identification and

823 quantification of shipping emissions in Bohai Rim, China, Sci. Tot. Environ., 497, 570-577, 2014.

824 Zhang, F., Wang, Z., Cheng, H., Lv, X., Gong, W., Wang, X., and Zhang, G.: Seasonal variations and

825 chemical characteristics of PM2.5 in Wuhan, central China, Sci. Tot. Environ., 518, 97-105, 2015.

826 Zhang, F., Chen, Y., Tian, C., Lou, D., Li, J., Zhang, G., and Matthias, V.: Emission factors for gaseous

827 and particulate pollutants from offshore diesel engine vessels in China, Atmos. Chem. Phys., 16, 6319-

828 6334, 10.5194/acp-16-6319-2016, 2016.

829 Zhang, M., Wang, X., Chen, J., Cheng, T., Wang, T., Yang, X., Gong, Y., Geng, F., and Chen, C.:

830 Physical characterization of aerosol particles during the Chinese New Year's firework events, Atmos.

831 Environ., 44, 5191-5198, 2010.

832 Zhang, R., Jing, J., Tao, J., Hsu, S. C., Wang, G., Cao, J., Lee, C. S. L., Zhu, L., Chen, Z., Zhao, Y., and

833 Shen, Z.: Chemical characterization and source apportionment of PM2.5 in Beijing: seasonal perspective,

834 Atmos. Chem. Phys., 13, 7053-7074, 10.5194/acp-13-7053-2013, 2013.

835 Zhang, X., Zhuang, G., Guo, J., Yin, K., and Zhang, P.: Characterization of aerosol over the Northern

836 South China Sea during two cruises in 2003, Atmos. Environ., 41, 7821-7836, 2007.

837 Zhao, B., Wang, S. X., Liu, H., Xu, J. Y., Fu, K., Klimont, Z., Hao, J. M., He, K. B., Cofala, J., and

838 Amann, M.: NOx emissions in China: historical trends and future perspectives, Atmos. Chem. Phys., 13,

839 16047-16112, 10.5194/acp-13-9869-2013, 2013a.

840 Zhao, M., Zhang, Y., Ma, W., Fu, Q., Yang, X., Li, C., Zhou, B., Yu, Q., and Chen, L.: Characteristics

841 and ship traffic source identification of air pollutants in China's largest port, Atmos. Environ., 64, 277-

842 286, 2013b.

843 Zhao, P. S., Dong, F., He, D., Zhao, X. J., Zhang, X. L., Zhang, W. Z., Yao, Q., and Liu, H. Y.:

844 Characteristics of concentrations and chemical compositions for PM2.5 in the region of Beijing, Tianjin,

845 and Hebei, China, Atmos. Chem. Phys., 13, 4631-4644, 10.5194/acp-13-4631-2013, 2013c.

846 Zhao, R., Han, B., Lu, B., Zhang, N., Zhu, L., and Bai, Z.: Element composition and source

847 apportionment of atmospheric aerosols over the China Sea, Atmos. Pollut. Res., 6, 191-201, 2015.

848 Zhao, X. J., Zhao, P. S., Xu, J., Meng, W., Pu, W. W., Dong, F., He, D., and Shi, Q. F.: Analysis of a

849 winter regional haze event and its formation mechanism in the North China Plain, Atmos. Chem. Phys.,

850 13, 5685-5696, 10.5194/acp-13-5685-2013, 2013d.

851 Zhou, D., Li, B., Huang, X., Virkkula, A., Wu, H., Zhao, Q., Qiao, Y., Shen, G., Ding, A., Zhang, J., Liu,

852   Q., Li, L., Li, C., Chen, F., and Yuan, S.: The Impacts of Emission Control and Regional Transport on

853   PM2.5 Ions and Carbon Components in Nanjing during the 2014 Nanjing Youth Olympic Games,

854   Aerosol. Air. Qual. Res., 17, 730-740, 10.4209/aaqr.2016.03.0131, 2017.

855   Zhou, M., Qiao, L., Zhu, S., Li, L., Lou, S., Wang, H., Wang, Q., Tao, S., Huang, C., and Chen, C.:

856   Chemical characteristics of fine particles and their impact on visibility impairment in Shanghai based on

857   a 1-year period observation, J. Environ. Sci. (China), 48, 151-160, 2016.

858   Zou, Y., Deng, X. J., Zhu, D., Gong, D. C., Wang, H., Li, F., Tan, H. B., Deng, T., Mai, B. R., and Liu,

859   X. T.: Characteristics of 1 year of observational data of VOCs, NOx and O3 at a suburban site in

860   Guangzhou, China, Atmos. Chem. Phys., 15, 6625-6636, 10.5194/acp-15-6625-2015, 2015.

861

Captions of Figure and Table

Table 1. The detailed information of $PM_{2.5}$ and $PM_{1.0}$ in the ambient during YRC.

Table 2. The pollutant levels and meteorological parameters in eight different episodes.

Table 3. The average concentration of the elements in $PM_{2.5}$ and $PM_{1.0}$ (ng m^{-3}) during YRC

Table 4. Comparisons of trace element concentrations with the reported data (μg m^{-3}).

Figure 1. Cruise tracks, source region limits, the sampling sites, and land use during YRC.

Figure 2. The average distribution of (a) aerosol optical depth at 550nm (MODIS L2); (b) CO column mixture ratio (MOPITT L2); (c) the SO_2 column concentration (OMI L2); (d) the NO_2 column concentration (OMI L2) over MLYR region.

Figure 3. Spatial concentration distributions of the soluble ions and levoglucosan in $PM_{2.5}$ along the cruise path.

Figure 4. Comparisons major ionic species during YRC with other regions, including: Beijing, Xi'an, Chengdu, Wuhan, Guangzhou, Shanghai, Northern South China Sea, Taiwan Strait, South China Sea, East China Sea and Tuoji Island. The red lines mark the sample routes in different cruises.

Figure 5. **(a)** Principal component analysis (PCA) of the typical elements in $PM_{2.5}$; **(b)** Time series of four typical element sources derived from PCA. All of the units are in μg m^{-3}.

Figure 6. Probable sources from PSCF for individual elements in $PM_{2.5}$ during YRC. The criteria are the mean concentration for all.

Figure 7. Time serious of V concentration (read column), estimates of primary $PM_{2.5}$ from ship emission, and number of ship distribution in the Yangtze River channel during YRC.

Table 1

Sample Number	Start data UTC	Day/Night Samples	Ship state	Sampling duration	Average Latitude, °N	Average Longitude, °E	PM$_{2.5}$ (μg m^{-3})	PM$_{1.0}$ (μg m^{-3})	PM$_{1.0}$/PM$_{2.5}$
#1	25-Nov-15	Daily	Moving	24 hours	30.95	117.78	63.83	58.30	91.33%
#2	26-Nov-15	Daily	Moving	24 hours	30.30	116.95	112.70	84.58	75.06%
#3	27-Nov-15	Daily	Moving	24 hours	29.73	115.86	106.40	90.37	84.96%
#4	28-Nov-15	Daily	Moving	24 hours	30.37	115.06	81.49	73.69	90.43%
#5	29-Nov-15	Daytime	Moving	12 hours	30.63	114.53	157.70	136.10	86.32%
#6	29-Nov-15	Nighttime	Stopping	12 hours	30.69	114.45	161.80	152.20	94.06%
#7	30-Nov-15	Daytime	Moving	12 hours	30.42	114.92	80.56	65.56	81.38%
#8	30-Nov-15	Nighttime	Stopping	12 hours	30.09	115.32	106.30	89.29	83.99%
#9	1-Dec-15	Daytime	Moving	12 hours	29.72	115.97	96.00	81.83	85.24%
#10	1-Dec-15	Nighttime	Moving	12 hours	30.32	116.89	92.02	82.86	90.04%
#11	2-Dec-15	Daytime	Moving	12 hours	31.08	117.96	122.80	85.17	69.34%
#12	2-Dec-15	Nighttime	Moving	12 hours	31.90	118.55	163.20	118.40	72.55%
#13	3-Dec-15	Daytime	Moving	12 hours	32.27	119.44	152.90	108.70	71.09%
#14	3-Dec-15	Nighttime	Moving	12 hours	31.95	120.27	133.90	105.60	78.89%
#15	4-Dec-15	Daytime	Moving	12 hours	31.70	121.18	146.10	111.80	76.57%
#16	4-Dec-15	Nighttime	Stopping	12 hours	31.38	121.60	131.20	102.70	78.27%

Table 2

Periods	Data and time (BST[a])	Latitude	Longitude	wind speed (m/s)	RH%	NOx (ppb)	SO$_2$ (ppb)	CO (ppb)	PM$_{2.5}$ (SN[b])	T/B
EP-1	2015/11/22 12:00 to 2015/11/23 18:00	31.28 to 32.22	121.23 to 119.55	3.01	88.95	65.51	6.32	443.91		1.59
EP-2	2015/11/25 12:00 to 2015/11/27 14:00	31.01 to 29.91	117.79 to 116.35	2.86	66.73	57.50	12.45	704.48	(#1,2)	0.81
EP-3	2015/11/27 14:00 to 2015/11/29 00:00	29.84 to 30.50	116.35 to 114.83	2.48	69.72	68.16	16.15	676.20	(#3,4)	1.49
EP-4	2015/11/29 00:00 to 2015/11/30 18:00	30.50 to 30.18	114.83 to 115.25	2.18	83.01	62.65	8.60	1030.25	(#5-7)	0.97
EP-5	2015/11/30 18:00 to 2015/12/01 20:00	30.18 to 30.02	115.25 to 116.66	2.32	79.64	51.92	11.66	989.75	(#8,9)	2.61
EP-6	2015/12/01 20:00 to 2015/12/02 20:00	30.02 to 31.67	116.66 to 118.40	3.84	74.67	31.00	4.09	1139.33	(10,11)	0.96
EP-7	2015/12/02 20:00 to 2015/12/03 20:00	31.67 to 32.32	118.40 to 119.73	5.39	44.91	23.73	7.87	1224.88	(#12,13)	1.00
EP-8	2015/12/03 20:00 to 2015/12/05 06:00	32.32 to 31.36	119.73 to 121.61	2.68	38.86	57.55	16.62	1061.46	(#14-16)	1.73

[a] Beijing standard time (GMT-8); T/B is ratio of toluene to benzene; [b] sample number in Table 1.

Table 3

Contents		Average	Max	Min	Median	SD[a]
Mg	$PM_{2.5}$	629.87	1487.67	135.69	589.13	358.57
	$PM_{1.0}$	328.57	699.09	17.26	359.42	213.44
Al	$PM_{2.5}$	863.87	2400.13	21.13	786.17	618.66
	$PM_{1.0}$	631.37	1894.40	100.78	473.46	483.74
K	$PM_{2.5}$	865.88	1723.87	368.51	805.73	367.14
	$PM_{1.0}$	771.80	1560.67	326.41	739.86	303.33
Ca	$PM_{2.5}$	2724.35	5657.60	391.54	2381.94	1729.51
	$PM_{1.0}$	1525.39	3371.73	108.21	1455.19	1108.03
V	$PM_{2.5}$	9.71	60.00	0.19	7.33	13.45
	$PM_{1.0}$	9.20	55.50	1.18	6.80	12.72
Cr	$PM_{2.5}$	22.29	62.67	2.16	16.73	16.51
	$PM_{1.0}$	21.67	48.17	2.67	22.74	13.31
Mn	$PM_{2.5}$	56.63	152.12	9.08	42.56	43.42
	$PM_{1.0}$	45.80	106.33	8.58	31.56	31.75
Fe	$PM_{2.5}$	1644.84	5188.18	38.87	860.40	1590.29
	$PM_{1.0}$	934.30	2616.83	46.74	516.37	850.12
Co	$PM_{2.5}$	0.82	2.88	0.00	0.48	0.75
	$PM_{1.0}$	0.62	1.67	0.07	0.26	0.53
Ni	$PM_{2.5}$	10.53	73.64	1.83	5.61	16.82
	$PM_{1.0}$	8.19	32.29	1.39	4.35	7.89
Cu	$PM_{2.5}$	18.79	49.87	4.07	17.66	11.28
	$PM_{1.0}$	15.21	37.07	3.70	12.32	7.87
Zn	$PM_{2.5}$	295.08	638.08	125.36	221.83	159.05
	$PM_{1.0}$	288.84	485.26	81.91	261.06	156.34
As	$PM_{2.5}$	37.33	107.17	0.87	31.50	28.14
	$PM_{1.0}$	41.73	111.85	12.46	30.70	32.00
Se	$PM_{2.5}$	6.08	12.18	2.70	5.78	2.57
	$PM_{1.0}$	6.48	11.04	3.07	6.40	2.76
Cd	$PM_{2.5}$	2.72	5.00	1.30	2.50	1.06
	$PM_{1.0}$	5.42	39.20	1.30	3.33	9.09
Tl	$PM_{2.5}$	0.32	0.90	0.00	0.29	0.22
	$PM_{1.0}$	0.41	0.89	0.14	0.35	0.23
Pb	$PM_{2.5}$	98.37	176.54	53.26	95.68	35.91
	$PM_{1.0}$	110.45	274.80	53.04	102.84	54.07

[a] SD is one standard deviation.

Table 4

	2015[a] (this study)	2003 (Zhang et al., 2007)	2011 (Zhao et al., 2015)	2013-2014 (Li et al., 2016)	2012-2013 (Lai et al., 2016)	2011 (Tao et al., 2014)	2012-2013 (Zhang et al., 2015)	2008-2009 (Huang et al., 2013)	2009-2010 (Zhao et al., 2013)
	Winter	Spring	Spring	Winter	Winter	Winter	Winter	Winter	Winter
	Yangtze River channel[b]	Northern South China Sea	East China sea	Taiwan strait	Guangzhou (rural)	Chengdu	Wuhan	Shanghai	Beijing
Al	0.86	0.31	3.28	3.00	0.21	0.43	–	0.64	1.03
Ca	2.72	0.82	2.40	2.00	0.11	0.26	2.27	0.72	1.85
Fe	1.64	0.32	1.37	1.30	0.16	0.61	1.42	0.56	1.55
Mg	0.63	0.11	0.83	2.40	2.30	0.16	0.61	0.26	0.57
As	0.04	–	0.01	–	–	0.02	0.04	0.02	0.01
Cd	0.00	–	–	–	–	0.00	0.01	–	–
Cr	0.02	0.03	–	0.60	–	0.01	0.01	0.02	0.01
Cu	0.02	–	0.01	–	0.03	0.03	0.03	0.04	0.04
Mn	0.06	–	0.01	0.70	0.03	0.07	0.13	0.04	0.09
Ni	0.01	–	0.01	0.90	–	0.00	0.01	0.01	0.01
Pb	0.10	0.16	0.02	0.70	0.09	0.20	0.24	0.06	0.15
V	0.01	–	0.02	–	–	0.00	–	0.01	–
Zn	0.30	–	0.07	0.60	0.27	0.32	0.37	0.13	0.30

[a] Sampling periods; [b] Sampling sites

Figure 1.
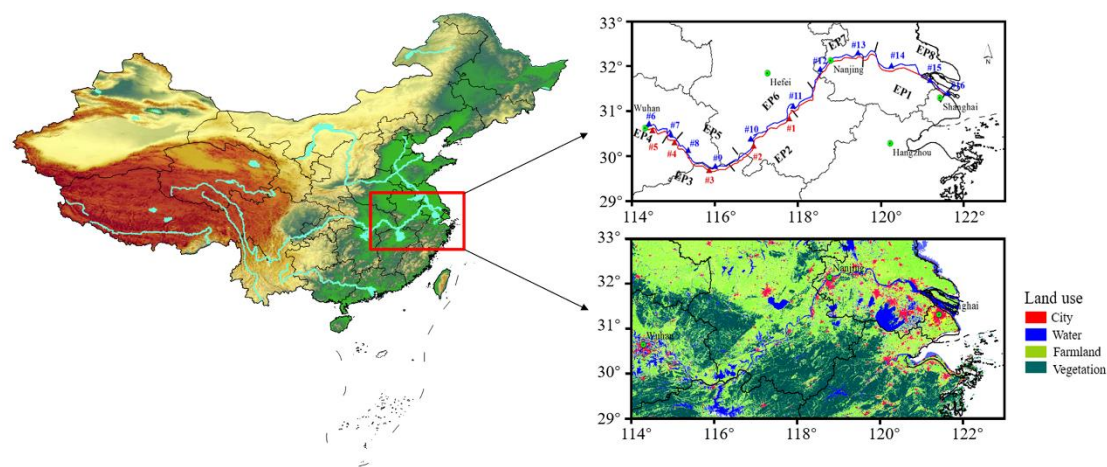
Figure 2.
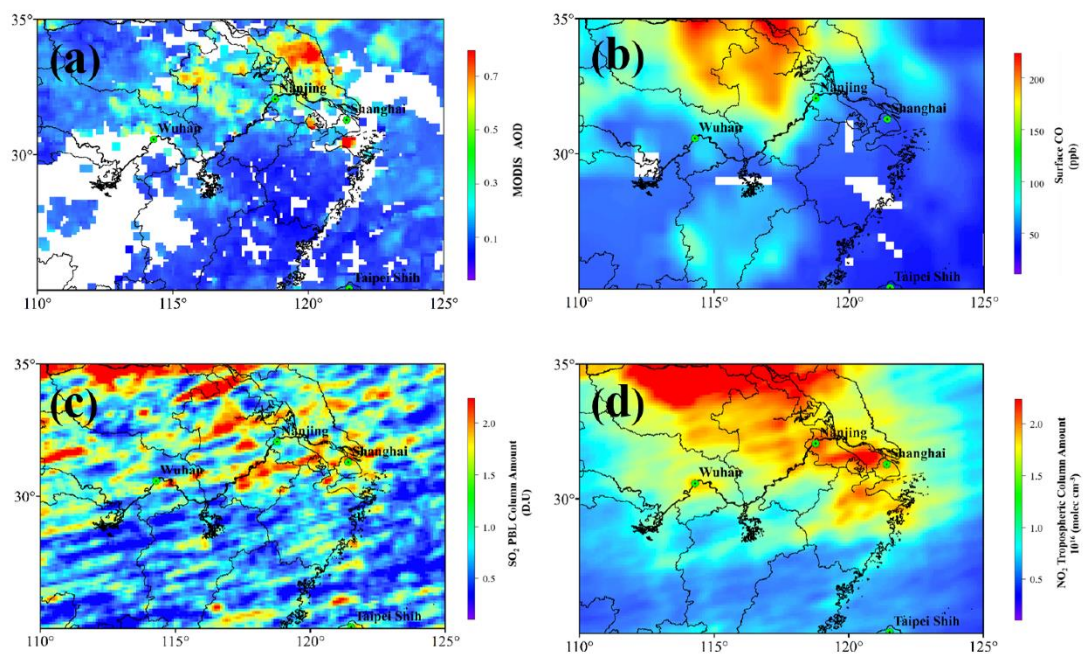
Figure 3.
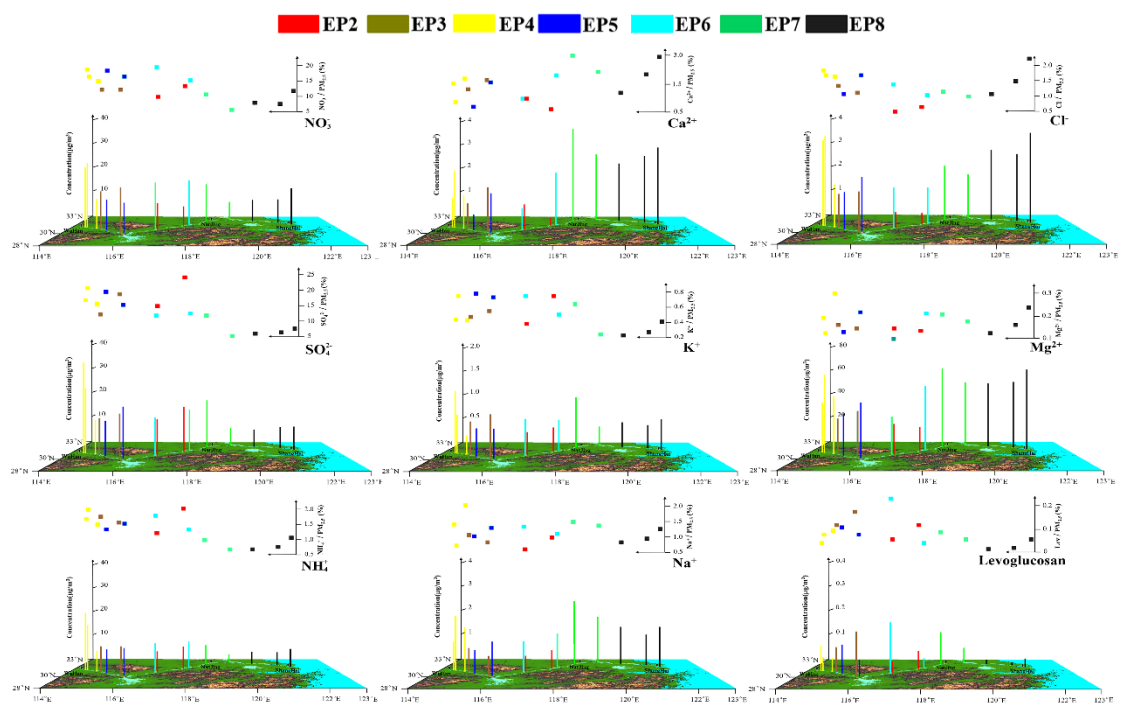
Figure 4.
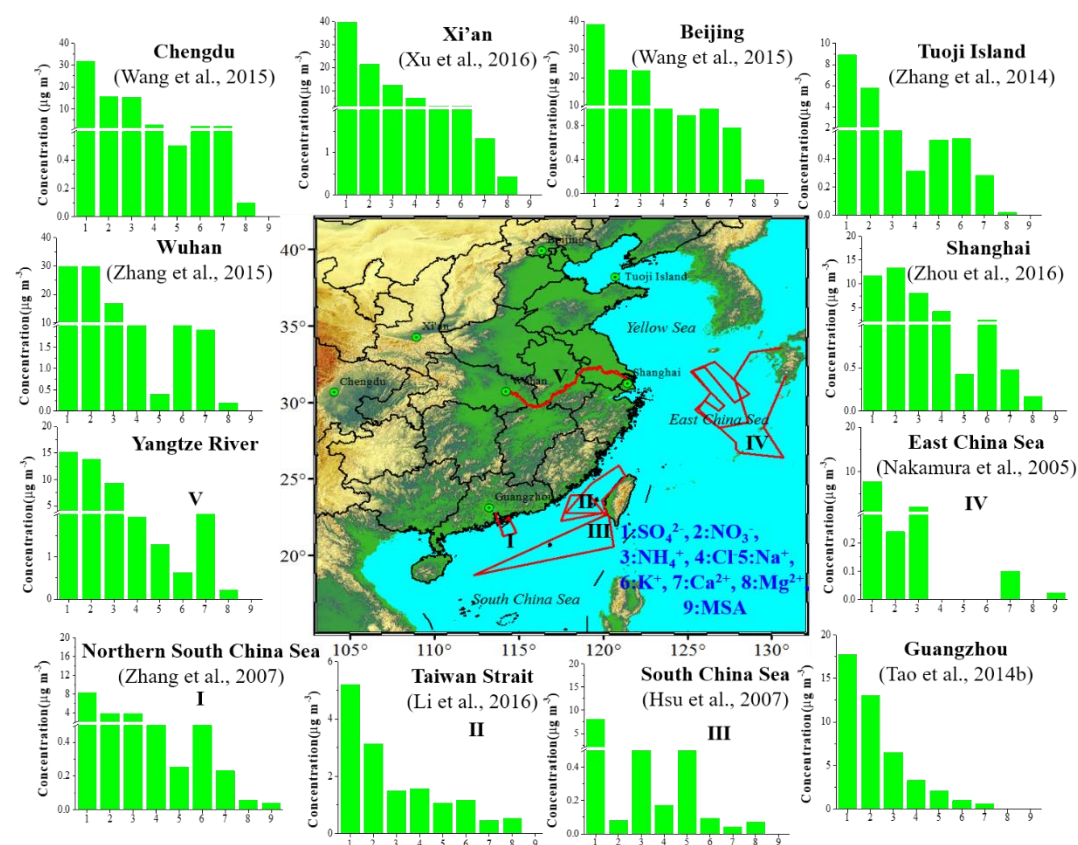
Figure 5.
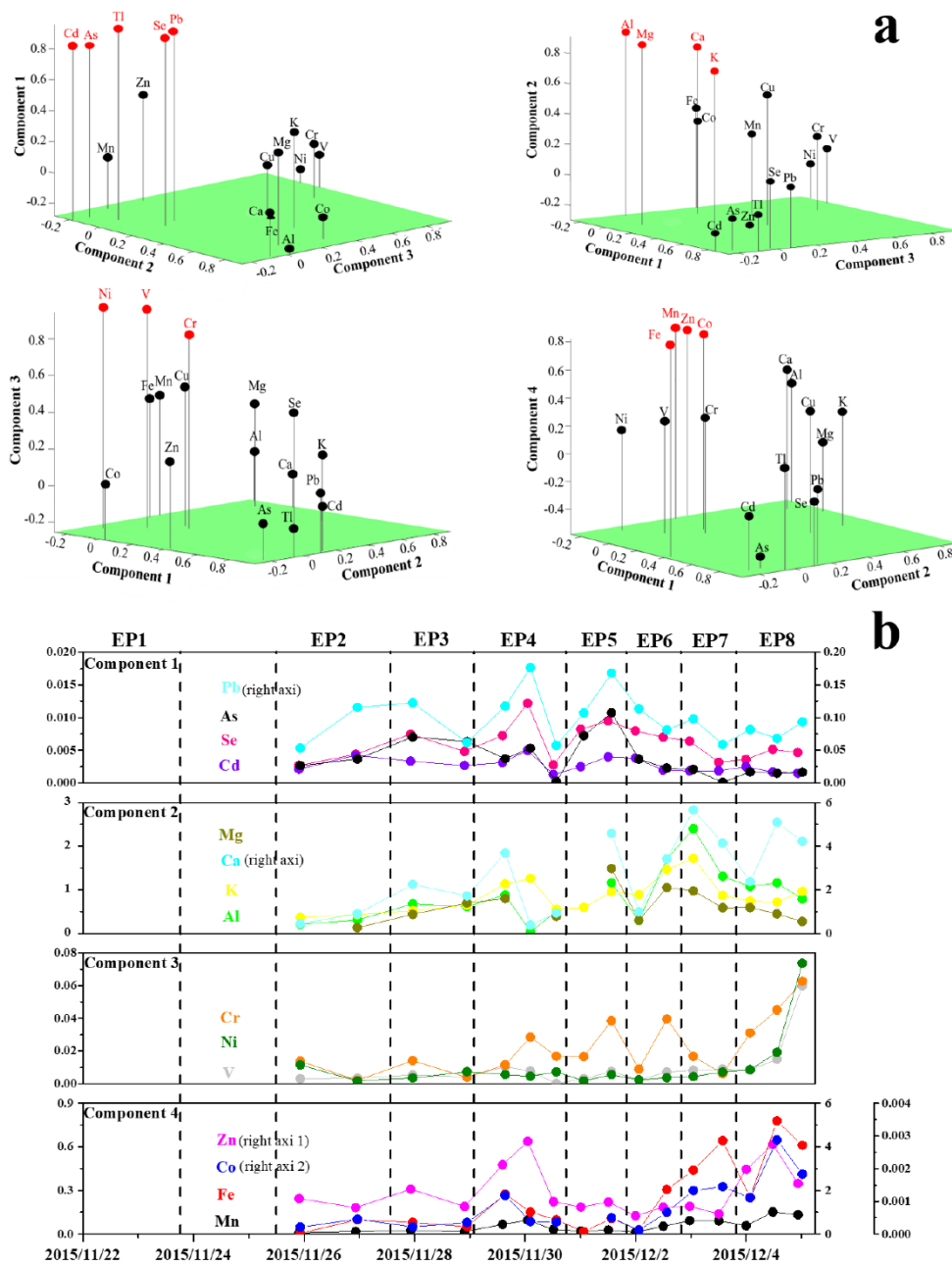
Figure 6.
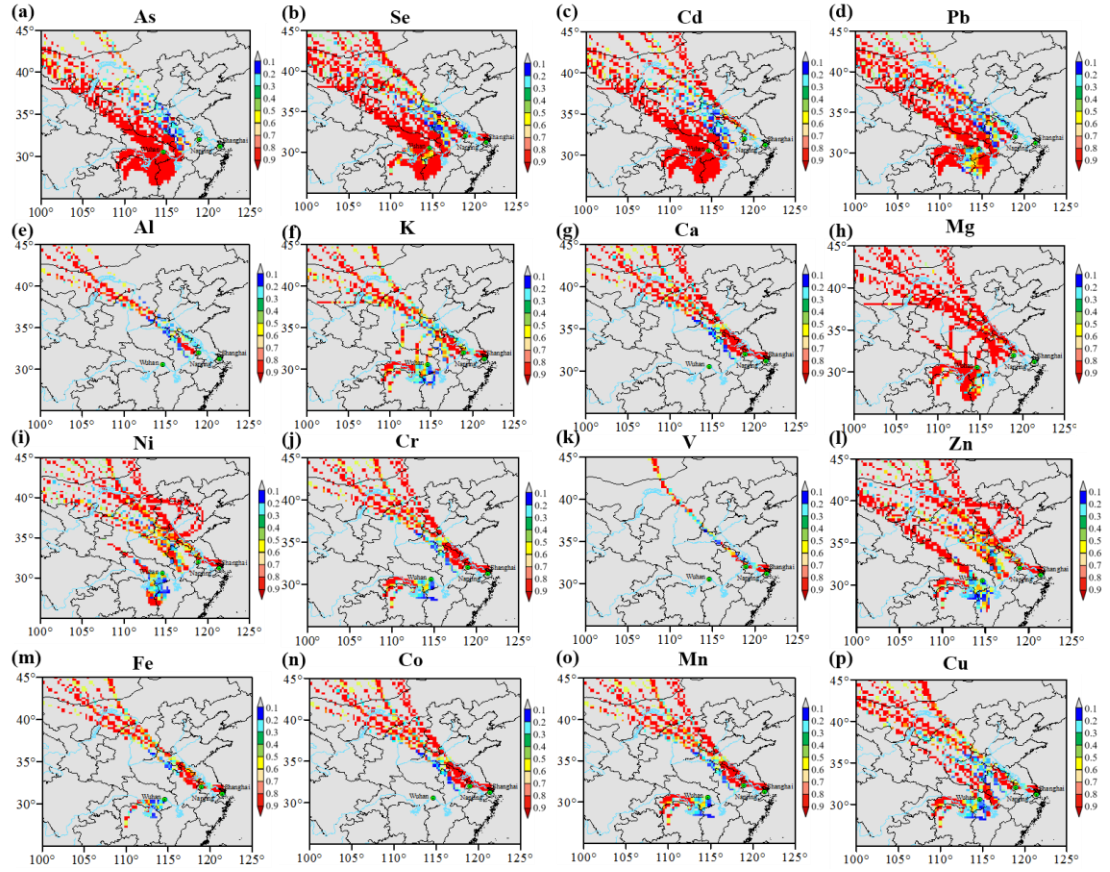
Figure 7.
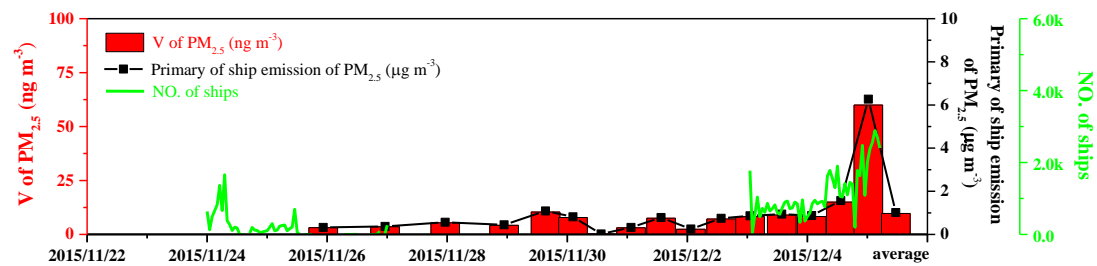
Supporting information:

Air quality in the middle and lower reaches of the Yangtze River channel: A cruise campaign

Zhong Li[1], Chunlin Li[1,2], Xingnan Ye[1], Hongbo Fu[1], Lin Wang[1], Xin Yang[1], Xinke Wang[3],Zhuohui Zhao[4], Haidong Kan[4], Abdelwahid Mellouki[5], Jianmin Chen[1,4,*]

[1] *Shanghai Key Laboratory of Atmospheric Particle Pollution and Prevention, Fudan Tyndall Center, Department of Environmental Science & Engineering, Institute of Atmospheric Sciences, Fudan University, Shanghai 200433, China*

[2] *Department of Earth and Planetary Sciences,Weizmann Institute of Science*

[3] *Univ Lyon, Université Claude Bernard Lyon 1 CNRS, IRCELYON, F-69626, Villeurbanne, France*

[4] *School of Public Health, Fudan University, Shanghai 200032, China*

[5] *Institut de Combustion, Aérothermique, Réactivité et Environnement, CNRS, 45071 Orléans cedex 02, France*

[*]Correspondence to*: **Jianmin Chen (jmchen@fudan.edu.cn)**

1 Meteorology pattern over the cruise

The MLYP region is located in East Asia Monsoon Region (China type), of which has a clear seasonal shift of the prevailing wind between in winter and summer. As shown in Figure S3, West Pacific Subtropical High (WPSH) control the south China in winter, while a cold high pressure formed in the north region of China during the period. During the sampling periods, WPSH was constantly squeezed further to south and ocean. The YRC region is completely situated between high pressure ridge and trough, thus northwest winds are dominant, as verified by two cold fronts on 25 November and 2 December in 2015, respectively. Besides, a low-pressure system formed in central China from 28 to 30 November, which was characterized by relative low wind speed and even stagnant air-mass, of which made a great contribution to the formation of the haze pollution (Huang et al., 2014;Huang et al., 2012).

The detailed meteorological information, including T, RH, pressure, wind speed and wind direction were monitored by an automatic meteorological station (HydroMet^{TM}, Vaisala) placed on the front of the vessel. The true wind, *i.e.*, a vector wind with a speed referenced to the fixed earth and a direction referenced to true north, was established by the platform-relative wind to ship and vessel speed, which was calculated directly from Global Positioning System (GPS) records (Smith et al., 1999). T and RH showed greatly changes during the survey, range from 1.05-18.90 ℃ and 26.90-99.00%, respectively. The surface wind direction was relative constant and wind speed was low in the most time during YRC, and the mean speed of 3.10 ± 0.99 m/s were measured. There were two sharp reduction of T and RH on 25 November and 2 December. When the cold front arrived, wind speed increases from 2 m/s up to 10 m/s.

Table S1. Emission factors of 11 metals from different fuel combustion (mg/kg) measured in our lab (Wu et al., 2017).

	Light diesel oil	Marine heavy oil	93 octane petrol	97 octane petrol
As	7.91 ± 1.03	1.77 ± 0.51	2.55 ± 0.31	1.30 ± 0.17
Fe	7.87 ± 1.12	12.28 ± 2.85	18.30 ± 1.39	20.07 ± 0.48
Al	4.39 ± 1.26	1.25 ± 0.35	0.33 ± 0.00	0.21 ± 0.00
Mn	2.62 ± 0.45	2.47 ± 0.70	0.57 ± 0.24	0.41 ± 0.03
Pb	1.13 ± 0.15	12.39 ± 0.65	ND	ND
Cr	0.73 ± 0.08	0.22 ± 0.09	0.24 ± 0.05	0.16 ± 0.10
Zn	0.43 ± 0.05	5.46 ± 1.32	0.05 ± 0.02	0.09 ± 0.03
Cu	0.40 ± 0.16	0.10 ± 0.03	0.40 ± 0.00	0.27 ± 0.12
V	ND	0.48 ± 0.11	ND	ND
Cd	ND	ND	ND	ND
Ni	0.24 ± 0.02	0.39 ± 0.06	0.07 ± 0.01	0.21 ± 0.04
TMs	25.72 ± 4.32	36.81 ± 6.67	22.51 ± 2.02	22.72 ± 0.97

Table S2. The average and maximum contribution of SO_4^{2-}, NO_3^-, OC and $PM_{2.5}$ from ship plume estimated by a lower limit ratio.

Ship emission contribution	$PM_{2.5}$	(OM/V) $_{min}$ = 290	(NO$_3^-$/V) $_{min}$ = 228	(SO$_4^{2-}$/V) $_{min}$ = 127
Average (μg m^{-3})	7.66	2.82	2.22	1.38
Maximum (μg m^{-3})	47.23	17.40	13.8	8.55
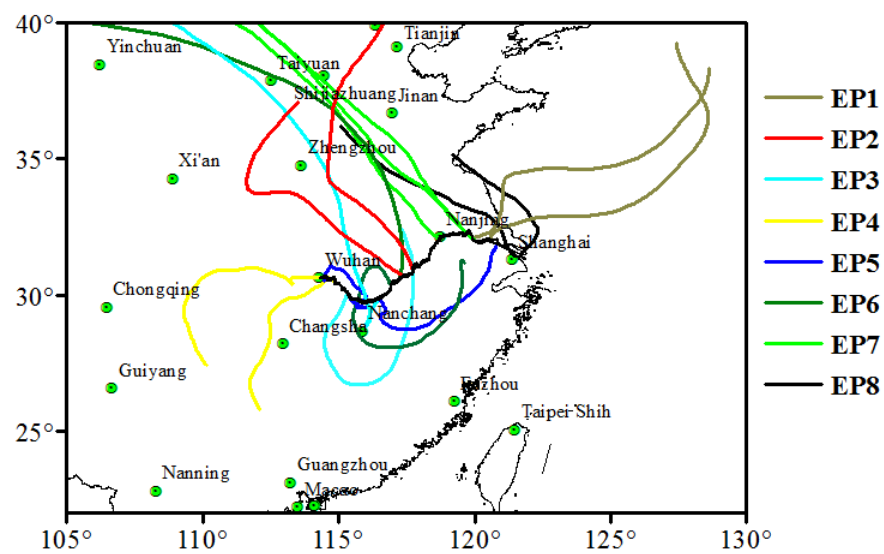
Figure S1. Ship route and 3-day back trajectories arriving at 500 m above sea level.
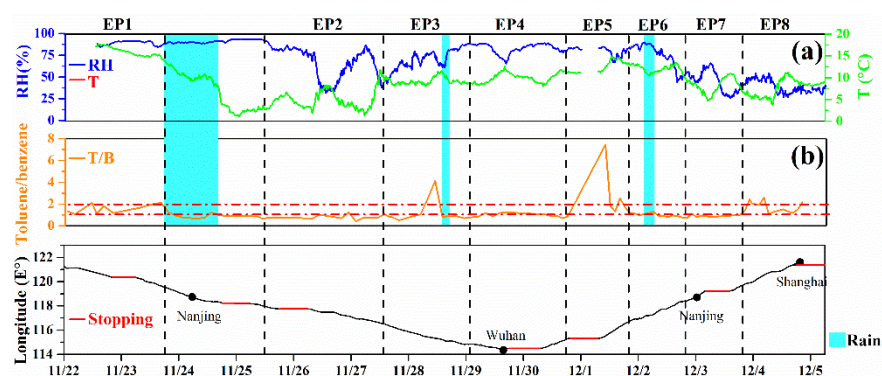
Figure S2. Time series of (a) meteorological parameters during YRC (T and RH); (b) ratio of

Toluene to Benzene.

862
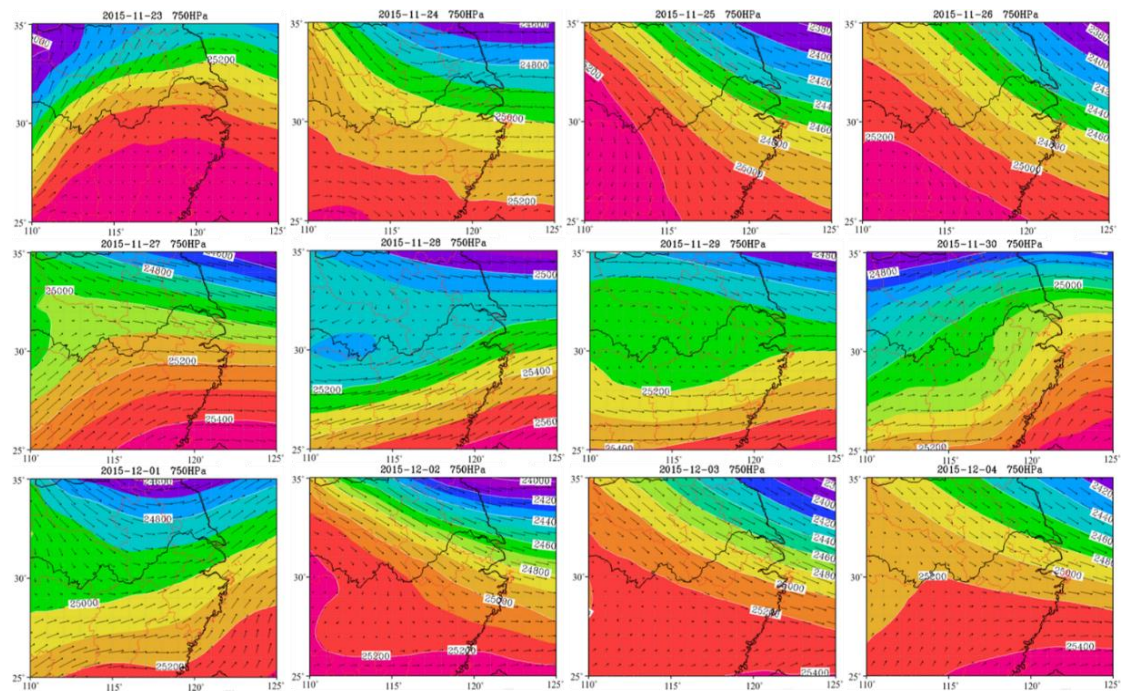
Figure S3. The average geopotential height field (white lines) and wind field (blank vector) for 750 hPa for each day during YRC.
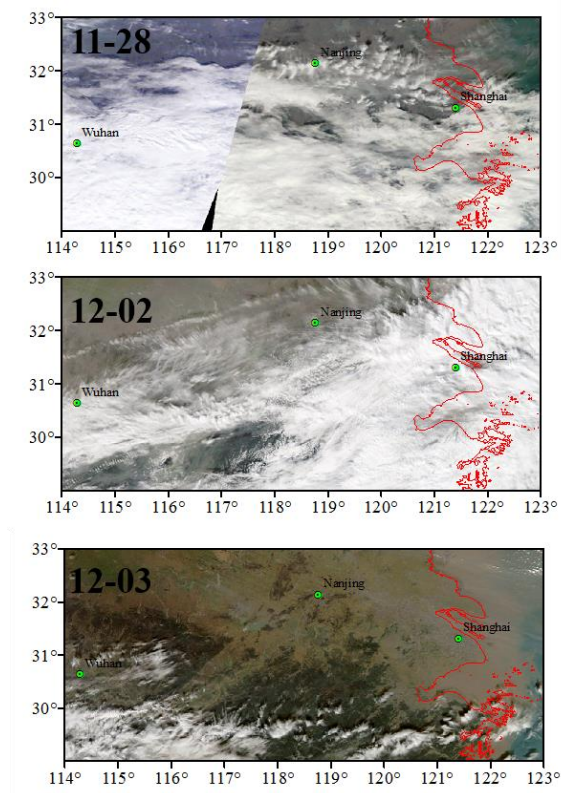
Figure S4. MODIS true-color imagery on 28 November, 2 and 3 December in 2015.
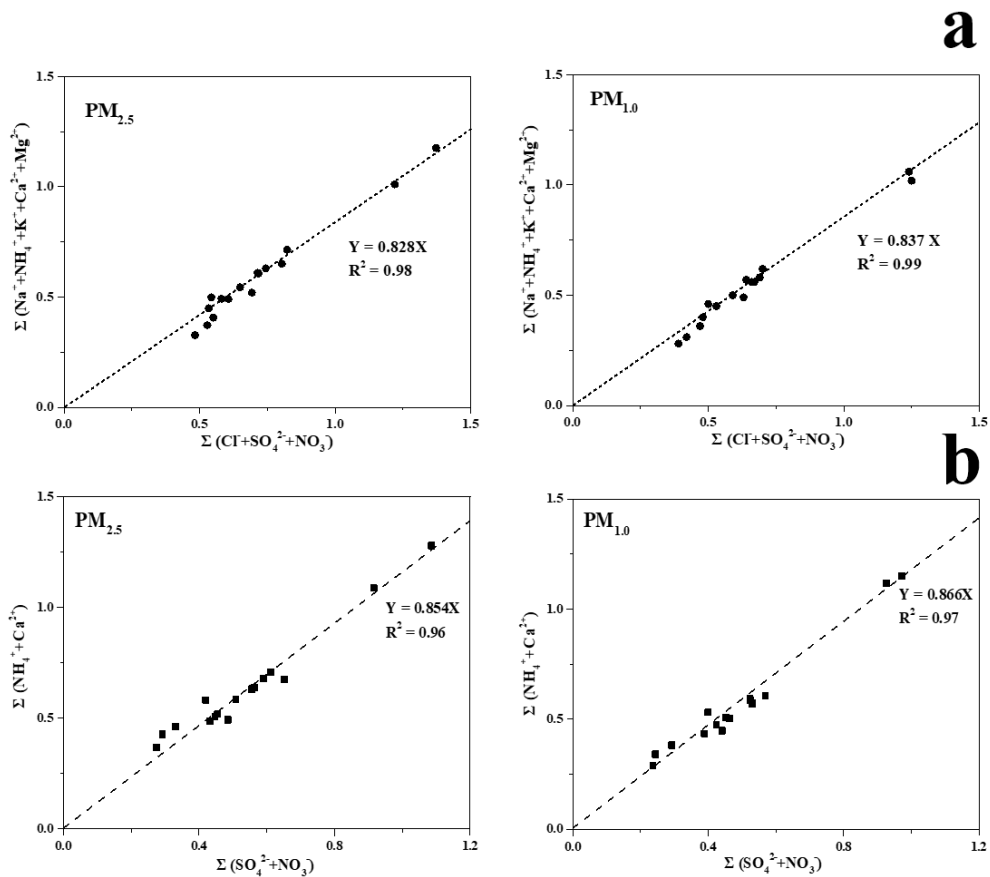
Figure S5. (a) The ion balance; (b) The correlation between the equivalent concentrations of

$[SO_4^{2-} + NO_3^-]$ and $[NH_4^+ + Ca^{2+}]$ in the present study (μ eq m^{-3}).
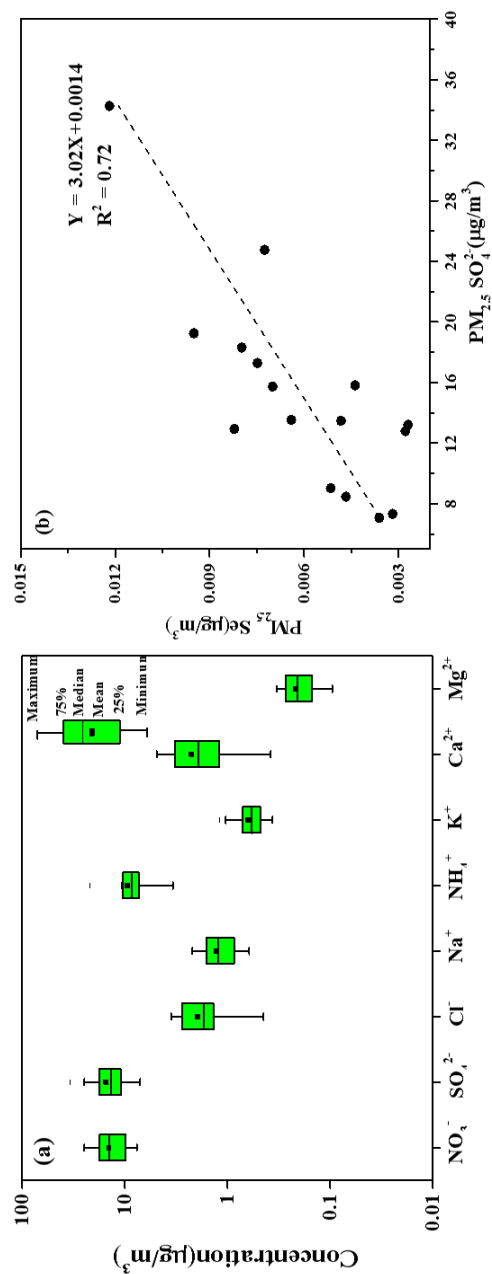
Figure S6. (a) average mass concentration of the main soluble ions along YRC; (b) the linear

correlation between Se and SO_4^{2-} in PM$_{2.5}$.
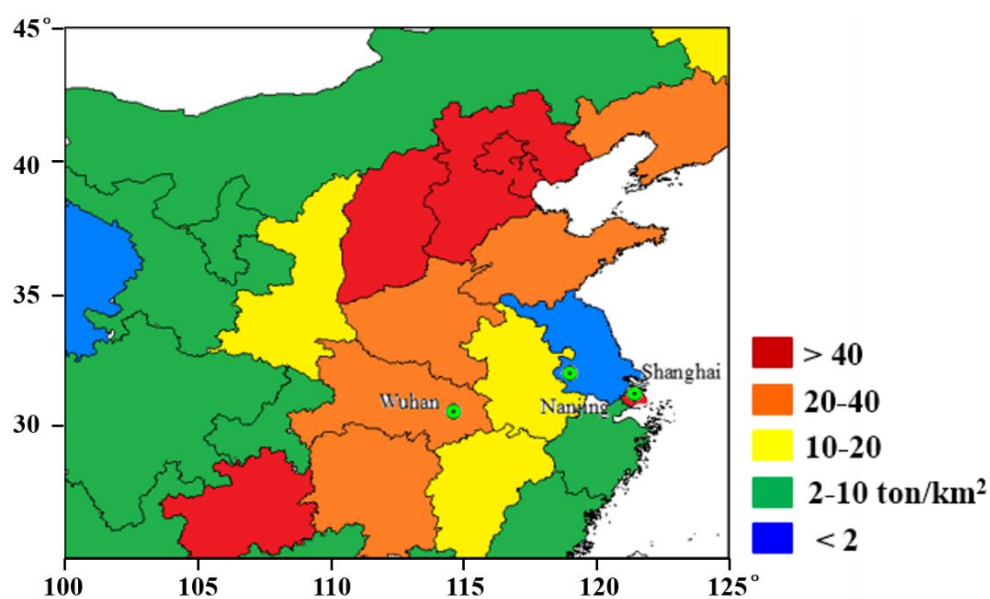
Figure S7. Residential coal consumption in China in 2015 (source: China energy statistical yearbook (NBSC, 2016)).
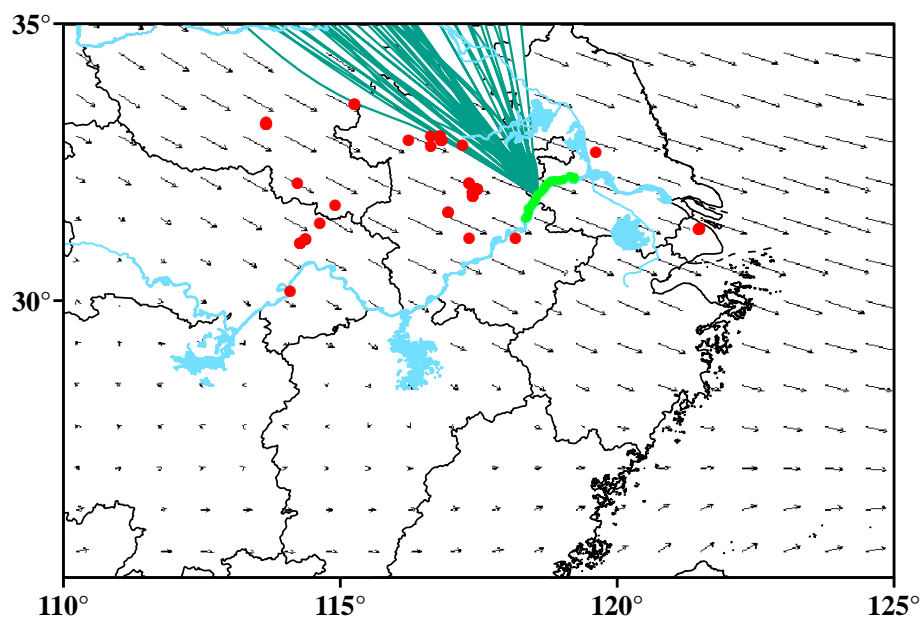
Figure S8. Mean wind vectors for sample #12 beginning at 18:00 LST and ending at 06:00 LST next day. Green line is the route for this sample. Red dots represent the FIRMS's fire points.
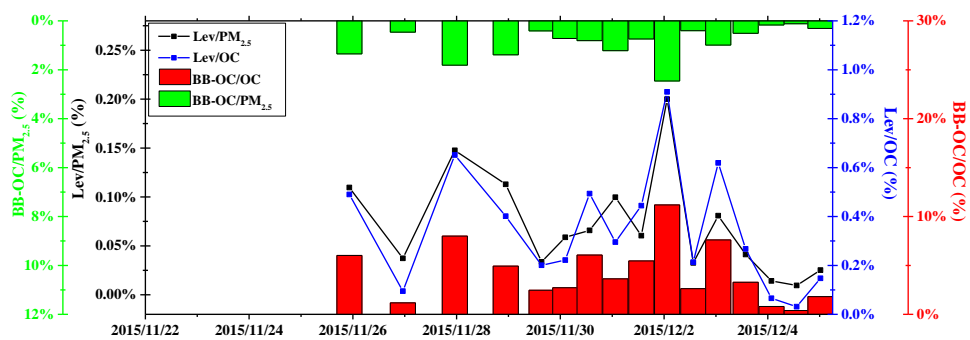
Figure S9. Time serious of Lev/OC and Lev/PM$_{2.5}$ ratios, and contribution of BB-OC to OC and PM$_{2.5}$ during YRC
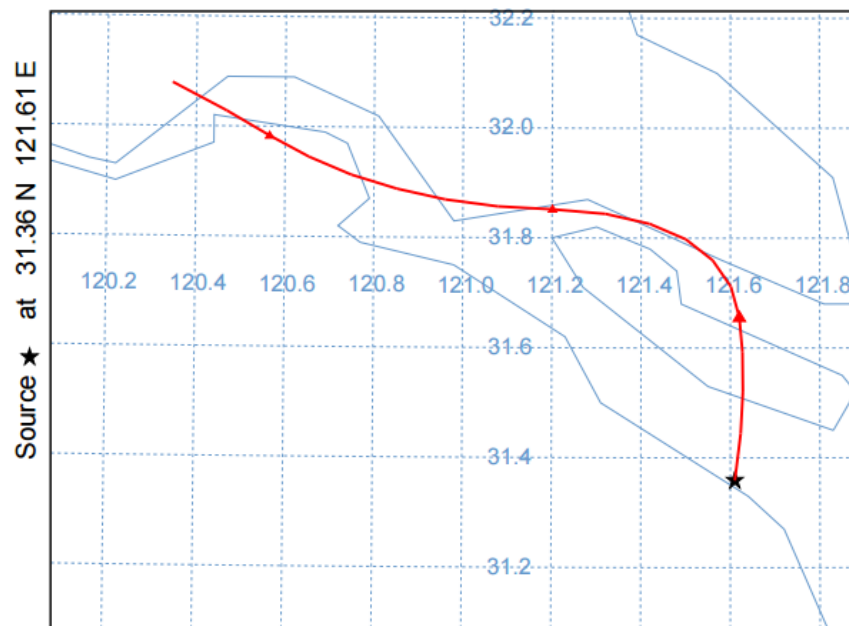
Figure S10. 18-hours back trajectories arriving at 500 m above sea level during the sample #16.
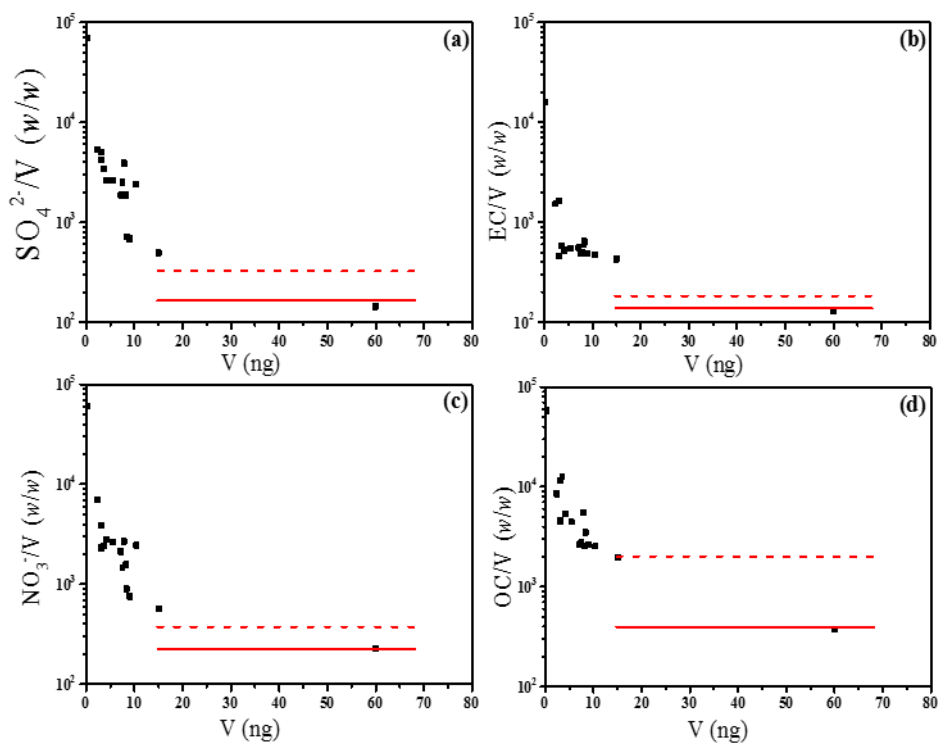
Figure S11. Scatter ration of (a) SO_4^{2-}/V, (b) NO_3^-/V, (c) EC/V and (d) OC/V along YRC. The red dashed line represented average ratio and solid line express the minimum ratio (average minus one standard deviation) for the sample with $V > 15$ ng/m^3.

Reference:

Huang, K., Zhuang, G., Lin, Y., Fu, J. S., Wang, Q., Liu, T., Zhang, R., Jiang, Y., Deng, C., and Fu, Q.: Typical types and formation mechanisms of haze in an Eastern Asia megacity, Shanghai, Atmos. Chem. Phys., 12, 105, doi: 10.5194/acp-12-105-2012, 2012.

Huang, R.-J., Zhang, Y., Bozzetti, C., Ho, K.-F., Cao, J.-J., Han, Y., Daellenbach, K. R., Slowik, J. G., Platt, S. M., and Canonaco, F.: High secondary aerosol contribution to particulate pollution during haze events in China, Nature, 514, 218-222, 2014.

NBSC: China energy statistical yearbook (2016) (in Chinese), China Statistics Press, 2016.

Smith, S. R., Bourassa, M. A., and Sharp, R. J.: Establishing more truth in true winds, J. Atmos. Ocean Tec., 16, 939-952, 1999.

Wu, D., Zhang, F., Lou, W., Li, D., and Chen, J.: Chemical characterization and toxicity assessment of fine particulate matters emitted from the combustion of petrol and diesel fuels, Sci. Tot. Environ., 605, 172-179, 2017.